

<https://doi.org/10.1038/s42003-025-09171-9>

# Medium-chain triglycerides and ketogenic diet prevent alterations of the gut microbiome in transgenic Alzheimer's disease mice

Check for updates

Paule E. H. M'Bra <sup>1,2,3</sup>, Isaura Suárez-Urbe <sup>1</sup>, Mariano Avino <sup>4</sup>, Evelyne Ng Kwan Lim<sup>5</sup>, Marian Mayhue<sup>1,2</sup>, Philippe Balthazar<sup>5</sup>, Anne Aumont<sup>1,2</sup>, Karine Prévost<sup>5</sup>, Eric Massé <sup>5</sup> ✉ & Karl J. L. Fernandes <sup>1,2,3</sup> ✉

The systemic mechanisms underlying the benefits of ketogenic interventions on cognition in Alzheimer's disease (AD) are understudied. Interventions involving a carbohydrate-free high-fat ketogenic diet (KD) or dietary supplementation with medium-chain triglycerides (MCT) both improve cognition in AD mouse models, yet with opposing effects on circulating ketones levels, peripheral insulin sensitivity and inflammation. Since the gut microbiome regulates systemic metabolism and inflammation and is altered by aging and disease, we investigated how it is affected in mice subjected to MCT and KD. At early stages of pathology, AD mice exhibited substantially reduced richness and distinct composition of gut microbiome species. Administration of MCT or KD for 1-month increased microbiome diversity, restoring the levels of more than 50% of the bacteria altered in AD mice and inducing novel alterations. Both diets increased levels of short-chain fatty acid-producing bacteria, such as *Lachnospiraceae*, which directly correlated with improved hippocampal dendritic spine density. Interestingly, longer term administration of KD increased the obesity-associated Firmicutes/Bacteroidota ratio and bodyweight in AD but not WT mice, suggesting that AD-associated metabolic defects should be considered when designing such intervention. We conclude that MCT and KD may influence AD central and peripheral defects in part via modulation of the gut microbiome.

Alzheimer's disease (AD) is characterized by pathological changes in the brain (amyloid plaques, neurofibrillary tangles, metabolic defects, and neuroinflammation) that lead to neuronal loss and progressive cognitive decline<sup>1–5</sup>. The exact pathogenesis of AD is not well understood. Sporadic AD, which is generally late-onset and represents 95% of all AD cases, is strongly influenced by systemic risk factors such as diabetes, obesity, inflammation and physical inactivity<sup>4,6</sup>. This suggests a key role for body-brain interactions in the etiology of AD.

Lifestyle interventions affecting peripheral metabolism, such as ketogenic dietary strategies, have yielded promising results in reducing mild cognitive impairment<sup>7</sup> and improving autonomy in patients with AD<sup>8</sup>. Ketone bodies, including acetoacetate and beta-hydroxybutyrate (BHB),

constitute a cell-permeable energy source for the brain that is preserved during aging and AD<sup>9</sup>. The classic low-carbohydrate, high-fat ketogenic diet triggers an energetic metabolic switch from glucose to the use of ketones derived from hepatic oxidation of fatty acids<sup>10</sup>. Given the challenge of long-term adherence to such a regime, dietary supplementation with ketogenic substrates such as medium-chain triglycerides (MCT)<sup>11</sup> composed of capric (C10:0) and caprylic (C8:0) acids<sup>12,13</sup> has been explored. Hepatic oxidation of these medium-chain fatty acids (MCFA) can increase blood ketones without the need for carbohydrate restriction<sup>14</sup>. Although dietary supplementation with MCT and adherence to a ketogenic diet can increase ketonemia and improve brain energy metabolism<sup>7,15–18</sup>, the observed cognitive benefits of such interventions are variable, with some non-responding patients<sup>18</sup>. This

<sup>1</sup>Department of Medicine, Faculty of Medicine and Health Sciences, Université de Sherbrooke, Sherbrooke, QC, Canada. <sup>2</sup>Research Center on Aging, CIUSSS de l'Estrie-CHUS, Sherbrooke, QC, Canada. <sup>3</sup>Department of Neurosciences, Faculty of Medicine, Université de Montréal, Montreal, QC, Canada. <sup>4</sup>Bioinformatic platform, Faculty of Medicine and Health Sciences, Université de Sherbrooke, Sherbrooke, QC, Canada. <sup>5</sup>Department of Biochemistry and Functional Genomics, Université de Sherbrooke, Sherbrooke, QC, Canada. ✉e-mail: [Eric.Masse@USherbrooke.ca](mailto:Eric.Masse@USherbrooke.ca); [Karl.Fernandes@USherbrooke.ca](mailto:Karl.Fernandes@USherbrooke.ca)

raises questions about the underlying mechanisms mediating the cognitive effects of such interventions, including their potential effects on peripheral tissues and systemic processes.

In this regard, we recently modeled the effects of ketogenic interventions in 3xTg-AD and 5xFAD transgenic mouse models of AD, showing that both an MCT-enriched carbohydrate-based diet (70% carbohydrates, 10% ketogenic MCT with C8:0/C10:0 ratio of 3:2) and a carbohydrate-free, high fat ketogenic diet (KD) modulated hippocampal gene expression and similarly improved hippocampal-dependent spatial learning and memory. Interestingly, despite their similar effects on the brain, MCT and KD interventions had vastly different effects on ketonemia and peripheral metabolism<sup>19</sup>; indeed, MCT did not increase circulating ketone levels yet improved the peripheral insulin sensitivity of AD mice, while KD induced a sustained elevation of circulating BHB, triggered pro-inflammatory liver gene expression and increased the adiposity of AD mice<sup>19</sup>.

Since gut bacteria are increasingly recognized for their roles in nutrient metabolism, immunity, neurological functions<sup>20,21</sup> and potential contributions to AD pathophysiology<sup>22–30</sup>, the present study investigated whether the gut microbiome of AD mice is remodeled by MCT and KD. Fecal levels of major microbial metabolites such as short-chain fatty acids (SCFA) decrease with aging and AD<sup>31,32</sup>, and altered microbiome features have been reported in transgenic mouse models of AD, suggesting links between aging, AD genetic risk and the gut microbiome<sup>33,34</sup>. Notably, the classic ketogenic diet and particularly production of BHB have been consistently shown to reduce a major type of fiber-digesting bacteria, *Bifidobacteria*, which support the growth of SCFA-producing bacteria through cross-feeding<sup>35,36</sup>. However, the reported effects of ketogenic diet on SCFA levels and SCFA-producing bacteria are controversial and might change according to the host physiological state<sup>35,37–39</sup>. Here, using stool samples from our well-studied prior cohorts of MCT- and KD-treated 3xTg-AD and 5xFAD mice, we evaluated whether these interventions modulated the effect of AD genetics on the gut microbiome and whether this might contribute to their observed cognitive benefits.

## Results

### KD, in contrast with MCT, induced a marked gut microbiome shift while inducing selective metabolic changes in AD mice

The gut microbiome of AD mice is reportedly altered even before the occurrence of cognitive deficits<sup>33,40</sup>, and is also highly influenced by age and diet. To examine the gut microbiome composition of wildtype (WT) and AD mice and changes as a result of MCT supplementation, KD, and diet duration, we sequenced the fecal microbiome of 3xTg-AD, 5xFAD, and their respective control mice at 1 or 2-month intervals beginning at pre-symptomatic stages (prior to cognitive deficits) (Fig. 1a, Supplementary Fig. 1a). 3xTg-AD mice, whose slow progression of amyloid plaques and neurofibrillary tangles facilitates study of pre-pathological stages<sup>41,42</sup>, were administered the diets for 5 months (from 3 to 8 months old). 5xFAD mice, a highly amyloidogenic fast-progressing model<sup>43</sup> useful for reproducing later stages of disease, were administered diets for 3 months (from 2 to 5 months old). Females were used because they present more severe brain pathologies and peripheral metabolic defects than males<sup>43,44</sup>.

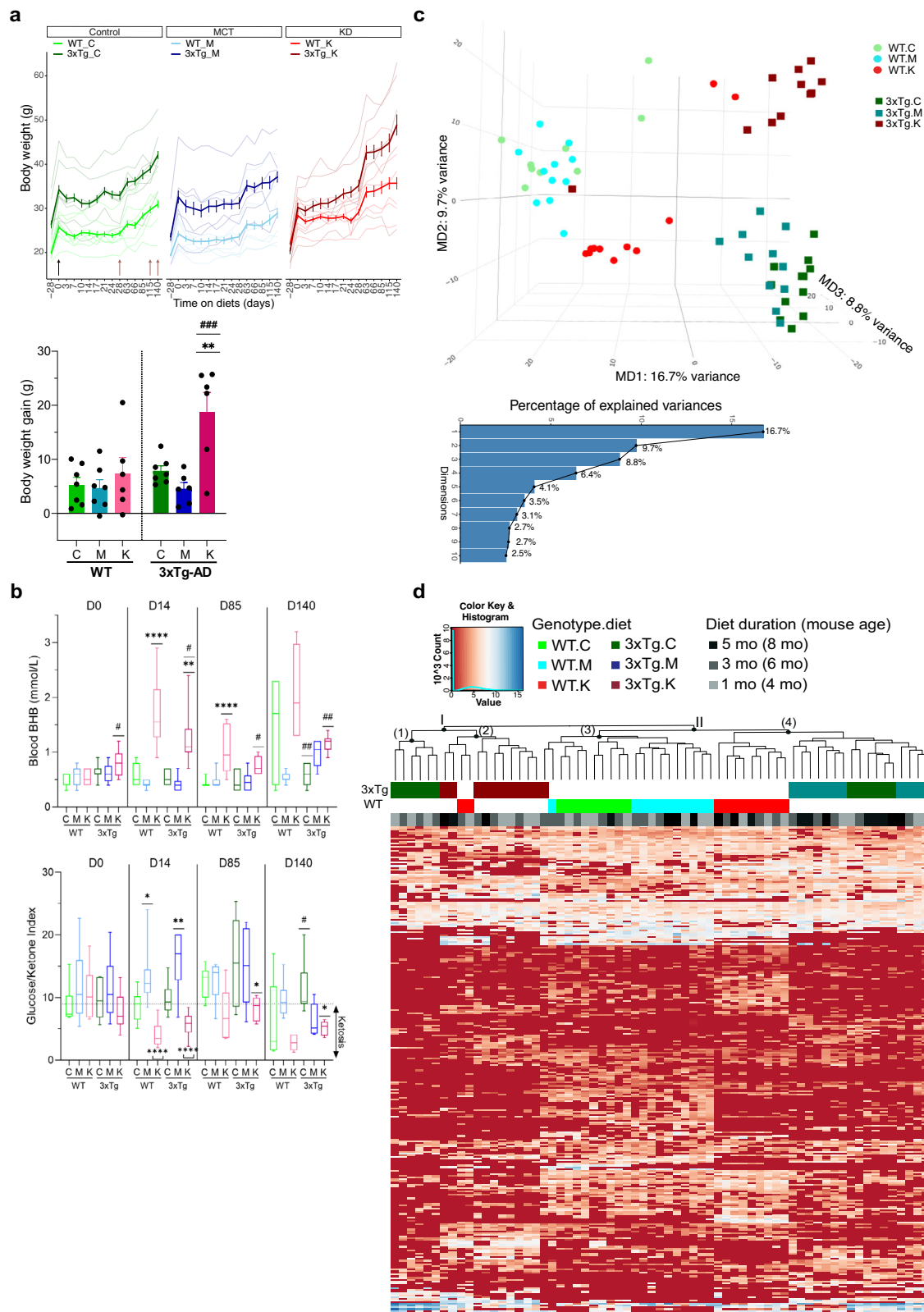
3xTg-AD mice, 5xFAD mice, and their aged-match WT counterparts were fed either a Control diet (70% carbohydrates, 20% fats (long-chain triglycerides), and 10% proteins, 4.1 kcal/g), an MCT-supplemented diet (70% carbohydrates, 20% fats (10% long-chain triglycerides, 10% medium-chain triglycerides), and 10% proteins, 4.1 kcal/g), or a KD (90% long-chain triglycerides and 10% proteins, 6.7 kcal/g), with all diets containing 50 g of fibers in the form of cellulose (Supplementary Table 1). The metabolic responses of the mice were assessed by measuring body weight, blood BHB and glycemia (Fig. 1a, b, Supplementary Data 1). All mice were on animal facility standard chow diet at baseline (28 days before diet and on day 0) (Fig. 1a, Supplementary Fig. 1a, Supplementary Table 1). 2 months-old (MO) 3xTg-AD mice exhibited higher body weight than WT mice (Fig. 1a—*days on diet: -28 to 0*). On Control and MCT diets, 3xTg-AD mice

remained similarly overweight compared to WT mice over the 5 months of diet, with similar weight gain from baseline (Fig. 1a—*days on diet: 0 to 140*). Interestingly, on the KD, 3xTg-AD mice exhibited strikingly more body weight gain than WT mice on KD or 3xTg-AD mice on Control diet (Fig. 1a—*Body weight gain*). 5xFAD mice at baseline had bodyweights that, unlike 3xTg-AD mice, did not differ or tended to be lower than their WT controls (Supplementary Fig. 1a—*days on diet: -28 to 0*). While the body weight gain of their WT strain was similar across the Control, MCT and KD diets (Supplementary Fig. 1a—*days on diet: 0 to 85*), 5xFAD mice on the KD had increased weight gain compared to Control and MCT diets such that their bodyweights overtook those of WT: from day 63 to day 85, 5xFAD mice on KD tended to weigh 2–3 g more than WT mice on the same diet (Supplementary Fig. 1a—*days on diet: 0 to 85*). Thus, despite model-specific variations, both 3xTg-AD and 5xFAD mice showed selective increases in body weight gain in response to the KD.

We assessed blood BHB concentration and the glucose/ketone index (GKI) as measures of hyperketonemia (BHB > 0.05 mmol/L and higher than BHB levels in mice fed the Control diet) and a ketosis state (GKI < 9), respectively. This revealed that KD stimulated hyperketonemia (Fig. 1b, Supplementary Fig. 1b) and a ketosis state (Fig. 1b, Supplementary Fig. 1b) in 3xTg-AD, 5xFAD mice, and their WT counterparts. However, AD mice exhibited a significantly lower KD-induced BHB increase compared to their WT controls, which was observed from day 14 in 3xTg-AD mice (Fig. 1b) and on day 85 in 5xFAD mice (Supplementary Fig. 1b). None of the mice fed with MCT showed changes in blood ketone levels or GKI, which remained the same as those of mice on the Control diet (Fig. 1b, Supplementary Fig. 1b). Thus, KD, but not MCT, triggered a sustained increase in blood BHB levels, with both AD mouse models showing a dampened ketogenic response versus WT, suggesting that AD genetics alter some metabolic functions.

We then analyzed the dissimilarities among the gut microbiomes using multidimensional scaling (MDS; Fig. 1c, Supplementary Fig. 1c), hierarchical clustering, and a heatmap of the relative abundance of the most representative amplicon sequence variants (ASVs; Fig. 1d, Supplementary Fig. 1d). After quality control, filtering, and phylogenetic classifications, we identified 283 ASVs for comparison in 3xTg-AD and WT mice fecal matter (Supplementary Data 2). MDS analysis showed a marked genotype effect, as visualized by the separation between 3xTg-AD and WT mice along the two main axes of the plot, which together captured 26.4% of the variability of the data (Fig. 1c—*MD1 and MD2*). The second main difference was among the dietary interventions. Mice fed the MCT and Control diets partially overlapped within their WT or 3xTg-AD genotypes, while mice on the KD prominently separated along the MD2 and MD3 axes that accounted for 9.7% and 8.8% of the variance respectively (Fig. 1c). Using the abundance patterns of the 283 ASVs and an unsupervised clustering method, mice separated into two clusters subdivided into four subclusters based on age, genotype and diet (Fig. 1d). Interestingly, the gut microbiome features of younger 3xTg-AD mice on Control diet (Fig. 1d—4, 6 MO, cluster I/subcluster 1) differed more than that of older 3xTg-AD mice on Control diet (8 MO, cluster II/subcluster 4) from the microbiome of WT mice (cluster II/subclusters 3,4) (Fig. 1d). This suggests that the baseline difference between 3xTg-AD and WT mice tends to decrease with aging with older 3xTg-AD mice converging toward WT mice. In addition, while 3xTg-AD mice on KD (cluster I/subcluster 2) were in the same cluster as younger 3xTg-AD mice on Control diet, the 3xTg-AD mice on MCT (cluster II/subcluster 4) clustered with WT and older 3xTg-AD mice on Control diet (Fig. 1d), indicating that 1-month MCT already shifts the 3xTg-AD microbiome toward that of WT mice.

The same analysis was performed for the 5xFAD model, in which 218 ASVs were identified for comparison. The MDS plot showed a significant diet effect of KD, with the microbiome of both 5xFAD and WT mice on KD separating from all mice on MCT and Control diet along the main axis (Supplementary Fig. 1c—*MD1 16.7% variance*). We noticed a clear distinction between 5xFAD and WT mice on KD that was not present on Control or MCT diets, suggesting an effect of AD genotype on the response



to KD (Supplementary Fig. 1c). Consistent with this, unsupervised clustering using the abundance patterns of 218 ASVs allowed the identification of two main clusters, separate into KD-fed mice (cluster I) and Control or MCT-fed mice (cluster II) (Supplementary Fig. 1d). The sub-clustering of KD-fed mice again highlighted a separation between WT (cluster I/sub-cluster 1) and 5xFAD mice (cluster I/subcluster 2) (Supplementary Fig. 1d).

Thus, while there was no baseline difference between WT and 5xFAD mice, they separated on the KD, suggesting AD genotype affects response to KD.

Altogether, these data reveal a model-specific microbiome composition, with baseline difference (WT vs AD mice) being more prominent in 3xTg model than 5xFAD model.

**Fig. 1 | KD, in contrast with MCT, induced a marked gut microbiome shift while inducing selective metabolic changes in 3xTg-AD mice.** **a** Body weight monitoring in mice fed diets ( $n = 6\text{--}7/\text{genotype}/\text{diet}$ ). The mixed-effect stats model identifies significant: Time effect ( $P < 0.0001$ ,  $F(2.518, 82.90) = 86.66$ ), genotype X diet effect ( $P = 0.0032$ ,  $F(5, 33) = 4.47$ ), Interaction effect (Time x Genotype X Diet,  $P < 0.0001$ ,  $F(12.59, 82.90) = 4.010$ ). The arrows indicate the start of the diet (black) and the time when fecal matter was harvested (brown). /Body weight gain at the end of diet (2-way ANOVA identifies genotype effect ( $P = 0.011$ ,  $F(1, 33) = 7.34$ ), diet effect ( $P = 0.001$ ,  $F(2, 33) = 8.53$ ) and interaction ( $P = 0.029$ ,  $F(2, 33) = 3.96$ )). Data are expressed as mean  $\pm$  SEM. **b** Blood levels of beta-hydroxybutyrate(BHB) and glucose/ketone index (GKI) at different timepoints. BHB: 2-way ANOVA at each time point shows at D0 (genotype effect:  $P = 0.01$ ,  $F(1, 33) = 7.46$ ), D14 (diet effect:  $P < 0.0001$ ,  $F(2, 33) = 30.25$ ), D85 (diet effect:  $P < 0.0001$ ,  $F(2, 33) = 16.26$ ), D140 (genotype effect:  $P = 0.017$ ,  $F(1, 33) = 6.31$ ), diet effect:  $P = 0.0009$ ,  $F(2, 33) = 8.68$ ), Interaction effect:  $P = 0.0055$ ,  $F(2, 33) = 6.13$ ). /GKI is the ratio of blood glucose levels out of blood BHB.  $GKI < 9$  indicates ketosis. 2-way ANOVA at each time point shows at D0 (not

significant), D14 (diet effect:  $P < 0.0001$ ,  $F(2, 33) = 25.45$ ), D85 (diet effect:  $P = 0.0023$ ,  $F(2, 33) = 7.34$ ), D140 (diet effect:  $P = 0.0041$ ,  $F(2, 33) = 6.52$ ), Interaction effect:  $P = 0.017$ ,  $F(2, 33) = 4.61$ ). Data are expressed as median and min/max, with boxplot identifying 25–75% range. Symbols illustrating significance on (a, b): Asterisks (\*) indicate significant diet effect (difference with Control diet) within the same genotype; Hashes (#) indicate significant genotype effect (difference with WT group) within the same diet. Statistical significance is presented on the graphs as follows: \* or #  $P < 0.05$ ; \*\* or ##  $P < 0.01$ ; \*\*\* or ###  $P < 0.001$ ; \*\*\*\* or ####  $P < 0.0001$ . **c** Multidimensional scaling (MDS) analysis of microbiome of experimental groups (65 samples,  $n = 3\text{--}4/\text{genotype}/\text{diet}/\text{time}$  excepted WT-C-5 months = 1) with percentage of variance explained, legend indicates genotype and diet. **d** Unbiased heatmap of all varying bacterial species abundance in fecal microbiome with hierarchical clustering of rows (283 ASVs) and columns (65 samples,  $n = 3\text{--}4/\text{genotype}/\text{diet}/\text{timepoint}$  excepted WT-C-5 months = 1), legend indicates genotype, diet, time and level of abundance.

In both models, KD prominently modulates microbiome composition while inducing changes in body weight and blood ketones levels, while MCT has more subtle effects.

### Gut microbiome diversity is reduced early in 3xTg-AD mice and partially reversed by MCT and KD

To begin investigating the microbiome features modulated by the dietary interventions, we explored the ASV-based alpha and beta diversities. Alpha diversity is a within-sample measure of the number of different species (richness) and their relative abundance (evenness of species representation)<sup>45</sup>. Beta diversity is a measure of diversity across samples, describing how similar or divergent two samples are<sup>45</sup>.

Alpha diversity was analyzed using three indices, namely Shannon describing the richness and evenness<sup>45</sup>, Chao1 for richness<sup>45</sup>, and Simpson for evaluating the presence of dominant species over the others<sup>46</sup> (Fig. 2a–c). These indices identified that younger 3xTg-AD mice on the Control diet (4, 6 MO) had significantly reduced alpha diversity compared to WT mice (Shannon, Fig. 2a; Chao1, Fig. 2c). MCT and/or KD interventions significantly increased the alpha diversity in 3xTg-AD mice, especially after 1 month of diet at 4 MO (Shannon, Simpson and Chao1, Fig. 2a–c). WT versus 3xTg differences in alpha diversity on the Control diet were less pronounced at older ages along with the impact of MCT and KD (Fig. 2a–c). We used three indices of beta-diversity: Bray-Curtis (based on relative abundance)<sup>47</sup>, Unweighted Unifrac (presence/absence of species and phylogenetic information)<sup>48</sup>, and Jaccard (presence/absence of species)<sup>47</sup>. These indices revealed marked dissimilarities between WT and 3xTg-AD mice on the Control diet at each time point with 3xTg-AD mice on MCT or KD tending toward WT mice on Control diet (Fig. 2d–f). However, Jaccard and unweighted Unifrac metrics indicated that the microbiome of 3xTg-AD mice on KD or MCT was not exactly aligned with WT mice microbiome (Fig. 2e, f). These results reveal that MCT and KD restore microbial alpha-diversity levels in 3xTg-AD mice to those seen in WT controls, but the specific microbial communities remain divergent (beta-diversity).

In the 5xFAD model, baseline alpha and beta diversity metrics of 5xFAD and WT mice on the Control diet did not differ significantly but after 1 month of intervention they were modulated by the diets specifically in the 5xFAD mice (Supplementary Fig. 2): the MCT diet reduced all alpha diversity indices in 5xFAD and the KD reduced the Chao1 index in 5xFAD mice, and these effects were not seen in the WT mice (Supplementary Fig. 2a–c). There were no significant differences in alpha diversity after 3 months of intervention (Supplementary Fig. 2a–c). All beta diversity metrics were consistent with a prominent diet-specific effect of KD in both WT and 5xFAD mice (Supplementary Fig. 2d–f).

Taken together, the microbiome diversity analysis revealed baseline alterations in alpha and beta diversities in 3xTg mice at early timepoints that declined with time and were absent in 5xFAD mice. MCT and KD partially prevented these changes in 3xTg-AD mice and induced selective alterations in 5xFAD mice.

### MCT and KD restored ASVs with differential abundance levels and induced new alterations in AD mice

We next performed differential abundance (DA) analyses at the ASV, family, and phylum levels in order to identify the bacterial differences between WT and AD mice at baseline and in response to MCT or KD.

Of the 283 identified ASVs, 102 were significantly different in abundance between WT mice and 3xTg-AD mice on the Control diet at 4 MO, with 87/102 being less abundant in 3xTg-AD mice and 15/102 being more abundant (Fig. 3a). The most abundant ASV in 3xTg-AD mice was *Bifidobacterium pseudolongum* (Fig. 3a—Log<sub>2</sub> fold change  $\approx 10$ ) and the least abundant were *Bacteroides thetaiotaomicron* and a species from the family *Muribaculaceae* (Fig. 3a—Log<sub>2</sub> fold change  $\approx -12$ ). The differentially abundant ASVs in 6 MO 3xTg-AD mice on the Control diet were reduced to 52 (Supplementary Fig. 3a—52 ASVs), with 83% (43/52) sharing the same expression pattern as in 4 MO mice (Fig. 3b). Strikingly, administration of the MCT and KD diets for 1 month at 4 MO corrected the relative abundance of 63/102 ASVs and 55/102 ASVs, respectively, including 41 that were reversed by both interventions (Fig. 3c, d). The proportion and type of ASVs corrected by MCT or KD remained similar after 3 months at 6 MO. (Supplementary Fig. 3b—22/52 ASVs with MCT, 30/52 ASVs with KD, Supplementary Fig. 3c). Besides correcting differentially abundant ASVs, MCT and KD also respectively altered the relative abundance of 17 and 51 additional ASVs (Fig. 3c). Thus, a substantial proportion of gut microbiome ASVs in young adult 3xTg-AD mice (4 MO, 6 MO) exhibit a major decrease in abundance while a few dominant ASVs increase in abundance, consistent with the previously described reduction in alpha diversity. MCT and KD partially reverse these alterations.

Phylum and family characterization performed in 4 MO mice revealed that 3xTg-AD mice on Control diet had higher levels of Actinobacteriota owing to the abundance of *Bifidobacterium pseudolongum* from the Bifidobacteriaceae family (Fig. 3e, f). Bacteroidota and Proteobacteria were globally in low abundance in 3xTg-AD mice on Control diet, mainly driven by decreased Muribaculaceae and Sutterellaceae families (Fig. 3e, f) while Verrucomicrobiota mainly composed of Akkermansia were not altered (Fig. 3e, f). Notably, although the overall Firmicutes levels were not altered, 3xTg-AD mice had reduced levels of Lachnospiraceae, Oscillospiraceae, Anaerovoracaceae, Oscillospirales UCG-010 families and increased levels of Lactobacillaceae (Supplementary Fig. 3d). Three Firmicutes with unidentified families were also altered in 3xTg-AD mice and belonged to the orders Clostridia UCG-014 and Clostridia vadin BB60 (Supplementary Data 2, Fig. 3d). Interestingly, 3xTg-AD mice presented a higher Firmicute:Bacteroidota ratio (F/B), an indicator of an altered microbiome generally observed in obesity phenotypes<sup>49–51</sup> (Fig. 3g).

Administration of MCT or KD for 1 or 3 months prevented the AD-induced phenotype by reducing levels of *Bifidobacterium pseudolongum* (Fig. 3d, Supplementary Fig. 3c) which significantly restored Bifidobacteriaceae and therefore Actinobacteriota levels (Fig. 3e, f). Both diets also

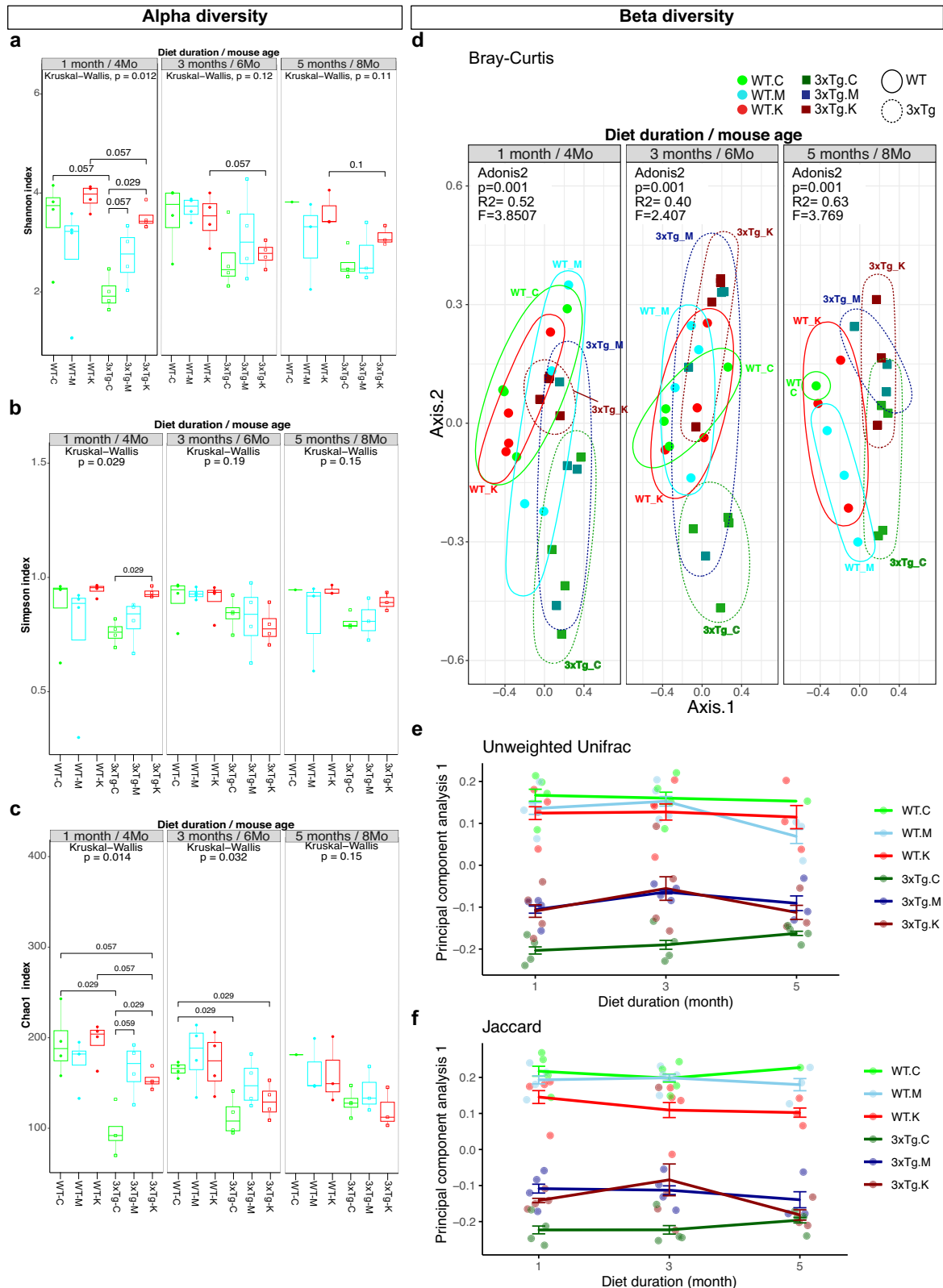
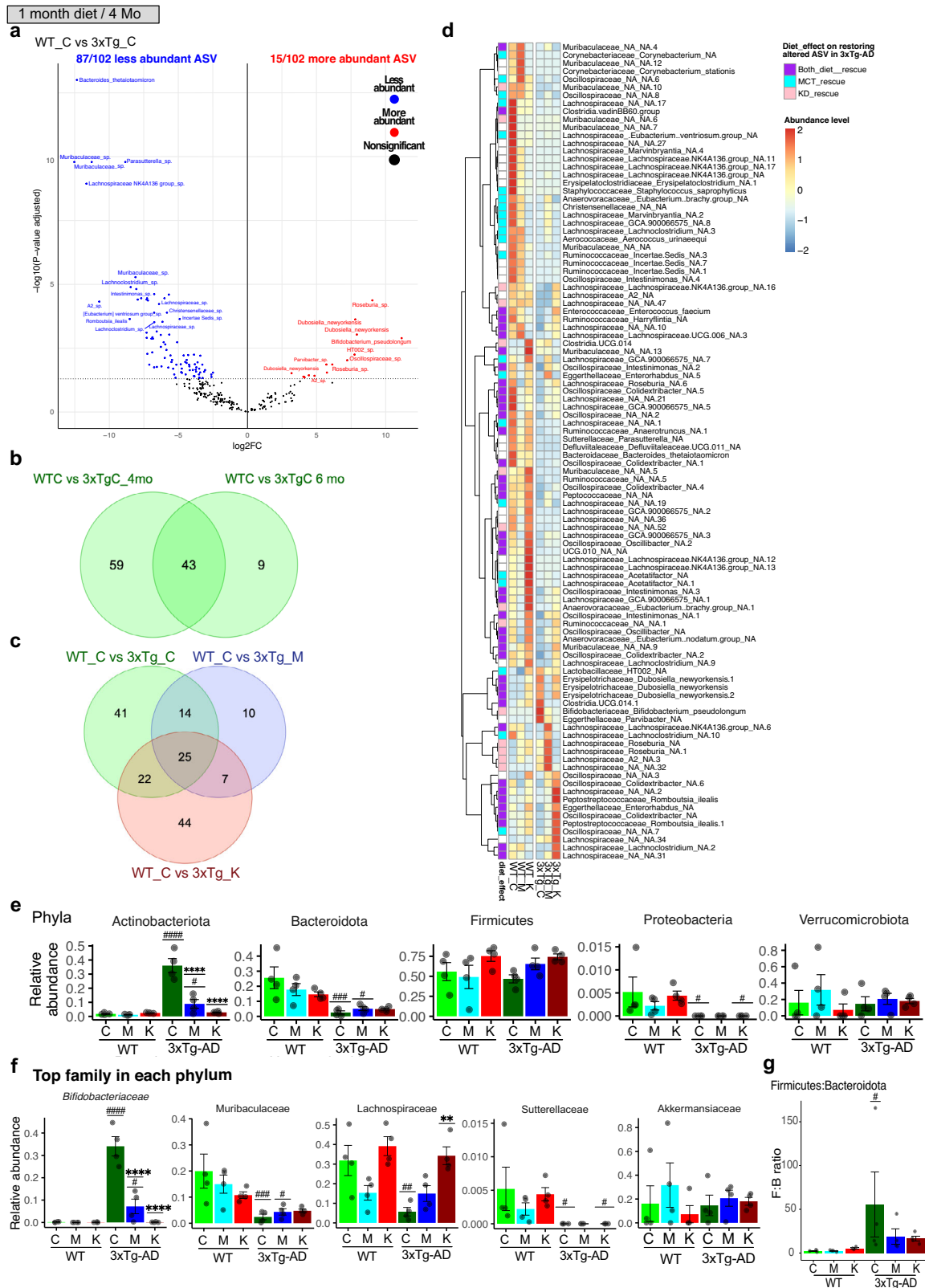


**Fig. 2 | 1-month of MCT and KD partially reversed lower gut microbiome diversity in 3xTg-AD mice.** Indices of Alpha diversity at different time points of the diet including **a** Shannon index, **b** Simpson index, and **c** Chao1 index (Multivariate statistical analysis with Kruskal-Wallis and pair-wise comparison post-hoc test: Wilcoxon, results on graph). Data are expressed as median and min/max, with boxplot identifying 25–75% range. **d–f** Indices of beta-diversity including: **d** Bray-

Curtis showing PCoA1 and PCoA2 (Multivariate statistical analysis with Adonis2 considering the following factors: group(genotypeXdiet) and residual, results for group factor on graph) **e** Volatility plot of the average changes of principal component analysis 1 (PCoA1) of Unweighted Unifrac distance matrix. **f** Volatility plot of the average changes of PCoA1 of Jaccard distance matrix. **e, f** Data are expressed as mean  $\pm$  SEM.



restored several Firmicutes families and introduced novel alterations in 3xTg-AD mice microbiome in diet-specific manner (Fig. 3f, Supplementary Fig. 3d). For instance, 1-month of MCT intervention restored overall Oscillospiraceae levels and several Lachnospiraceae species (Supplementary Fig. 3c, d, Fig. 3d) while introducing more Erysipelotrichaceae and Clostridiaceae in 3xTg-AD mice (Supplementary Fig. 3c, d).

KD restored overall levels of Lachnospiraceae and Anaerovoracaceae (Fig. 3d, e, Supplementary Fig. 3c, d) and added more Erysipelotrichaceae (Supplementary Fig. 3d). Most Bacteroidota and Proteobacteria remained unchanged by diet (Fig. 3d–f, Supplementary Fig. 3c, d).

In the 5xTg model, DA analysis identified only eight ASVs that were altered at 3 MO (Supplementary Fig. 4a, b) and only one at 5 MO

**Fig. 3 | 1-month of MCT or KD restored ASVs with differential abundance levels and induced new alterations in 3xTg-AD mice microbiome.** **a** Volcano plot of ASVs relative abundance fold change between WT and 3xTg-AD mice on Control diet (WT\_C vs 3xTg\_C,  $n = 4$ /genotype/diet, Limma adjusted  $P < 0.05$ ). **b** Venn diagram comparing differential ASVs in 4 months-old 3xTg-AD mice (WTC vs 3xTgC\_4mo,  $n = 4$ /genotype/diet, Limma adjusted  $P < 0.05$ ) and 6 months-old 3xTg-AD mice (WTC vs 3xTgC\_6mo,  $n = 4$ /genotype/diet, Limma adjusted  $P < 0.05$ ). **c** Venn diagram of the following comparisons ( $n = 4$ /genotype/diet, Limma adjusted  $P < 0.05$ ): AD-induced alterations (WT\_C vs 3xTg\_C), MCT effect in AD mice (WT\_C vs 3xTg\_M), KD effect in AD mice (WT\_C vs 3xTg\_K). The ASVs that are significantly different in WT\_C vs 3xTg\_C and not significant in WT\_C vs 3xTg\_M or WT\_C vs 3xTg\_K are considered “restored”. **d** Hierarchical heatmap of the average abundance of ASVs with differential abundance in WT\_C vs 3xTg\_C ( $n = 4$ /genotype/diet, adjusted  $P < 0.05$ ). The color code in the extreme left column indicates whether the ASV abundance is rescued by MCT (cyan), KD (pink), or both diets (purple). Asterisks indicate most and least abundant ASVs in 3xTg\_C compared to WT\_C. **e** Relative abundance of phyla. 2-way ANOVA identifies in Actinobacteriota (genotype effect:  $P < 0.0001$ ,  $F(1, 18) = 51$ , diet effect:  $P < 0.0001$ ,

$F(2,18) = 26$ , interaction effect:  $P < 0.0001$ ,  $F(2,18) = 27$ ), Bacteroidota (genotype effect:  $P < 0.0001$ ,  $F(1, 18) = 28.11$ ), Firmicutes (diet effect:  $P = 0.044$ ,  $F(2, 18) = 3.74$ ), Proteobacteria (genotype effect:  $P = 0.0034$ ,  $F(1, 18) = 11.33$ ) and Verruromicrobiota (not significant). **f** Relative abundance of the most abundance family in each phylum. 2-way ANOVA identifies in Bifidobacteriaceae (genotype effect:  $P < 0.0001$ ,  $F(1, 18) = 57.37$ , diet effect:  $P < 0.0001$ ,  $F(2,18) = 32.97$ , interaction effect:  $P < 0.0001$ ,  $F(2,18) = 32.47$ ), Muribaculaceae (genotype effect:  $P = 0.0003$ ,  $F(1, 18) = 19.66$ ), Lachnospiraceae (genotype effect:  $P = 0.015$ ,  $F(1, 18) = 7.16$ , diet effect:  $P = 0.0006$ ,  $F(2, 18) = 11.59$ , interaction effect:  $P = 0.034$ ,  $F(2, 18) = 4.11$ ), Sutterellaceae (genotype effect:  $P = 0.0034$ ,  $F(1, 18) = 11.33$ ), Akkermansiaceae (not significant). **g** Ratio of Firmicutes out of Bacteroidota relative abundance (F:B ratio). 2-way ANOVA identifies genotype effect ( $P = 0.048$ ,  $F(1,18) = 4.48$ ). Symbols illustrating significance on (e-g): Asterisks (\*) indicate significant diet effect (difference with Control diet) within the same genotype; Hashes (#) indicate significant genotype effect (difference with WT group) within the same diet. Statistical significance is presented on the graphs as follow: \* or #  $P < 0.05$ ; \*\* or ##  $P < 0.01$ ; \*\*\* or ###  $P < 0.001$ ; \*\*\*\* or ####  $P < 0.0001$ . Data are expressed as mean  $\pm$  SEM.

(Supplementary Fig. 4e), which is consistent with the similar microbiome diversity of 5xFAD and WT mice on the Control diet (Supplementary Fig. 2). At the phylum level, this corresponded to higher levels of Proteobacteria associated with Enterobacteriaceae at 3 MO, such as *Escherichia coli* (*Shigella*) (Supplementary Fig. 4a, Supplementary Fig. 5a, c). MCT and KD restored all 6/8 and 8/8 altered ASVs, respectively (Supplementary Fig. 4b). The only ASV altered in 5 MO 5xFAD mice was the most abundant ASV, a *Muribaculum* species (Supplementary Fig. 4a, Supplementary data 2), and this ASV was restored by both diets during both periods (Supplementary Fig. 4a, b). Interestingly, when exposed to the MCT or KD, the microbiome of 5xFAD mice showed specific changes, especially in Firmicutes and Verruromicrobiota, that were not observed in WT mice (Supplementary Fig. 5a–c). After 1 or 3 months of intervention, MCT tended to decrease the levels of Firmicutes more in 5xFAD mice than WT mice (Supplementary Fig. 5a–c), primarily affecting Lachnospiraceae and Oscillospiraceae (Supplementary Fig. 4c, e, Supplementary Fig. 5c). KD increased Firmicutes and decreased Verruromicrobiota in 5xFAD mice and did the opposite in WT mice (Supplementary Fig. 4d, f, Supplementary Fig. 5a); this resulted in a significant increase in the F/B ratio in 5xFAD mice fed the KD compared to WT mice fed the same diet (Supplementary Fig. 5b). Notably, *Akkermansia muciphila*, the most common Verruromicrobiota in the microbiome, was significantly reduced by KD in 5xFAD mice (Supplementary Fig. 4d, f, Supplementary Fig. 5c).

Taken together, genetic models of AD present (i) altered abundances of bacteria that are shifted towards normal by MCT and KD, and (ii) evidence of additional MCT or KD effects on the microbiome that specific to mice carrying AD mutations.

### Functional mechanisms associated with changes in the microbiome of 3xTg-AD mice fed with MCT or KD

We used PICRUST in order to predict functional changes associated with the microbiome composition of 3xTg-AD mice fed a Control diet and treated with dietary interventions for 1 month. We used two databases, Metacyc and KEGG, to derive metabolic pathway profiles and then performed a Pearson correlation analysis to highlight the ASVs driving these predicted functional changes.

Principal component analysis (PCA) on the predicted metabolic pathway profiles obtained with Metacyc revealed a baseline distinction between WT and 3xTg-AD mice on the Control diet along axis 2 (PC 2, Fig. 4a). 3xTg-AD mice on MCT or KD were more similar to the WT mice fed the Control diet along the same axis (PC 2, Fig. 4a), and most mice fed the KD were separated from those fed the MCT diet on axis 1 (PC1, Fig. 4a), indicating that genetics and diet both drive the differential metabolic pathways. 80 pathways with Metacyc and 21 pathways with KEGG were predicted to change across the six experimental groups (Fig. 4b, c, Supplementary Fig. 6a, b). These pathways were separated into three main

groups according to the dendrograms and their expression: (1) pathways reduced by MCT or KD in 3xTg-AD mice, (2) pathways increased by MCT or KD, and (3) pathways altered in 3xTg-AD mice with no diet effect (Fig. 4b, c).

For the first group, Metacyc and KEGG analyses revealed 26 pathways that were enriched in 3xTg-AD mice on the Control diet and reduced in 3xTg-AD mice on the MCT or KD. These pathways were related to amino acids (protein digestion and absorption, synthesis of aspartate-derived amino acids (L-lysine, L-threonine, L-methionine), L-alanine biosynthesis, and proteasome), carbohydrates (carbohydrate digestion and absorption, sucrose and glucose degradation), and synthesis of DNA precursors (pyrimidine and inosine monophosphate biosynthesis) (Fig. 4b, c, Supplementary Fig. 6a, b). The precursors of all these pathways are produced in the reductive tricarboxylic acid (TCA) pathway<sup>52,53</sup>, which was also enriched in 3xTg-AD mice but was unaltered by MCT or KD (Fig. 4b). In addition, KEGG predicted increased lipid mechanisms in 3xTg-AD on Control diet which were reduced with MCT or KD, such as PPAR signaling, fatty acid degradation, adipocytokine signaling (Fig. 4c, Supplementary Fig. 6b). In the same line, Metacyc highlighted increased *Bifidobacterium shunt* (Fig. 4b) and lactate production from hexose, also occurring in *Bifidobacteria*<sup>53,54</sup>.

The second group involved functions predicted to be increased by the microbiome of KD- or MCT-fed mice. Both databases highlighted a decrease in lipid biosynthesis in the microbiome of 3xTg-AD mice fed the Control diet, notably fatty acid biosynthesis, phospholipid biosynthesis, diacylglycerol, and phosphatidylglycerol (Fig. 4b, c, Supplementary Fig. 6a, b). These pathways were upregulated by the KD (Fig. 4b, c). 3xTg-AD mice fed MCT and/or KD had a microbiome enriched with ketone bodies or short-chain fatty acid (SCFA)-producing processes, including butanoate, acetoacetate and acetone production from the fermentation of pyruvate, acetyl-CoA, and L-lysine, as well as propionate formation from propane-diol degradation (Fig. 4b). Pathways involved in ketone body substrates or SCFA substrates were also increased with MCT or KD, such as L-lysine biosynthesis and fatty acid beta-oxidation (Fig. 4b), as well as processes of *Clostridium acetobutylicum* acidogenic fermentation for pyruvate synthesis and degradation into SCFA (Fig. 4b). Both diets resulted in a predicted increase of urea cycle and purine degradation (Fig. 4b). KD, but not MCT, increased various pathways of glycolysis and sucrose degradation, several arginine- and polyamine-related pathways and UDP-N-acetylmuramoyl-pentapeptide critical for peptidoglycan biosynthesis of gram-positive bacteria (Fig. 4b).

In the last group, approximately 12 pathways were predicted to be reduced in 3xTg-AD mice on the Control diet and remained unaffected by dietary interventions, with the most significant being related to apoptosis (Fig. 4c, Supplementary Fig. 6b), mannan degradation, chondroitin degradation, and inositol degradation (Supplementary Fig. 6a, Fig. 4b).

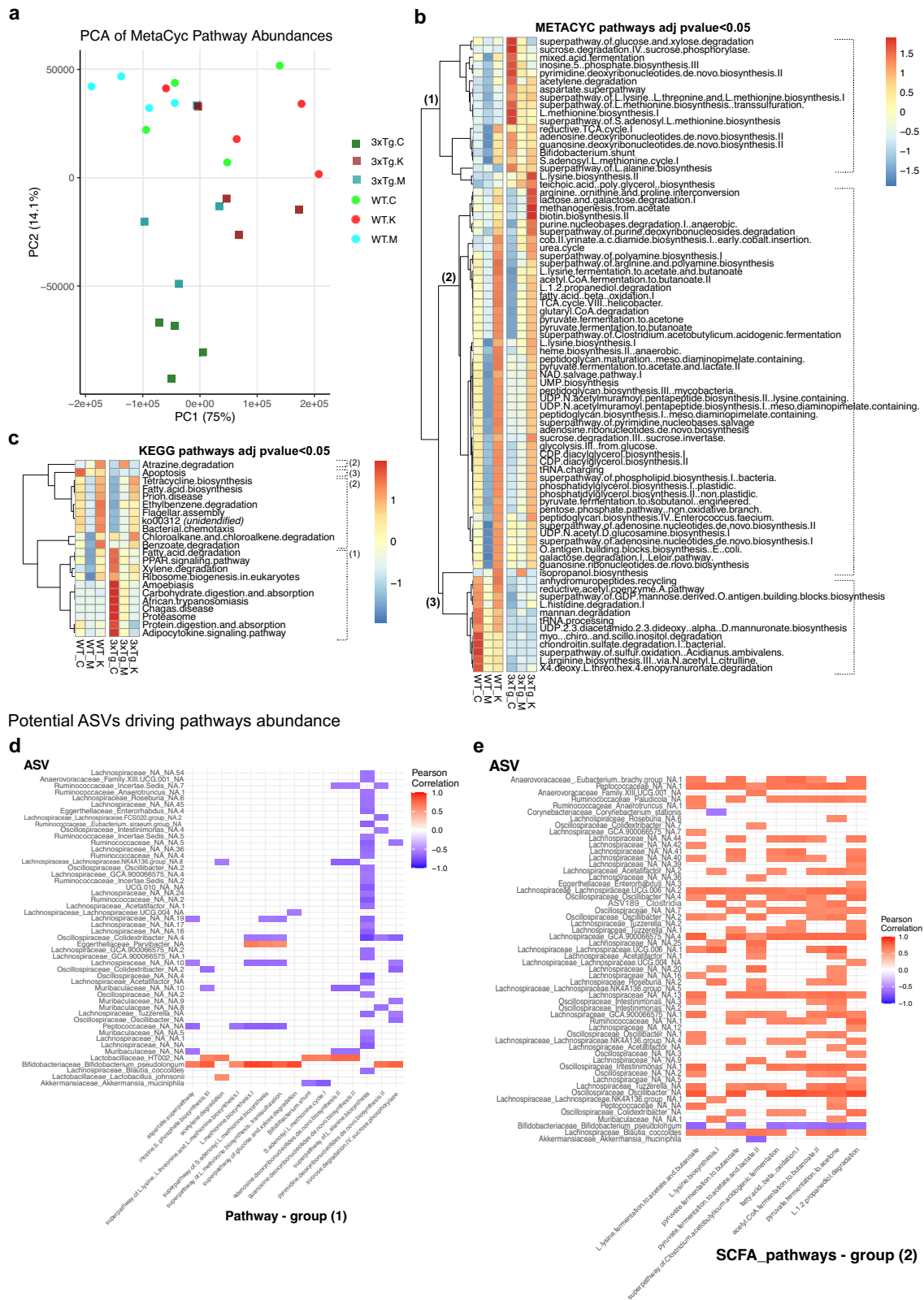
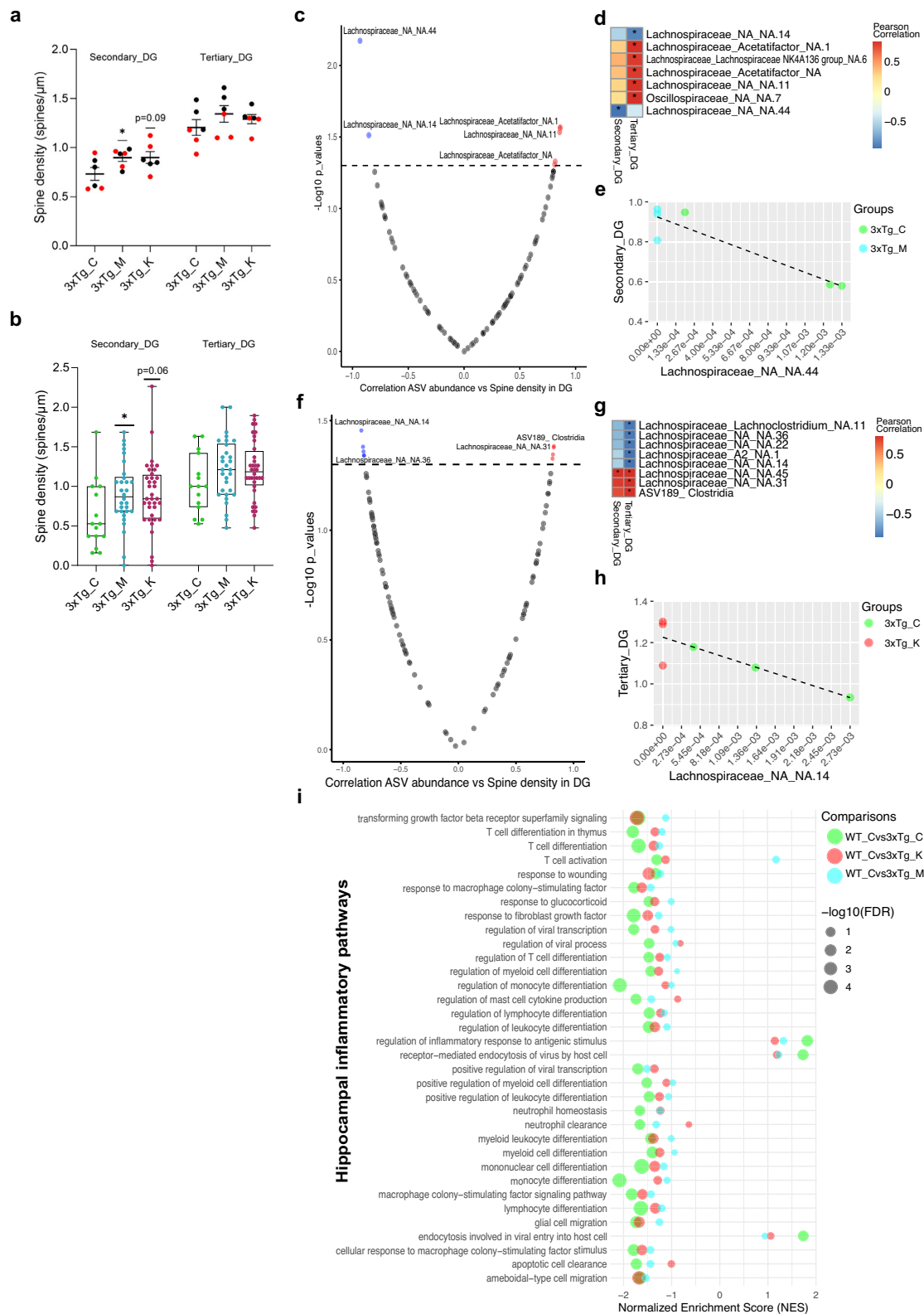


**Fig. 4 | Functional mechanisms associated with changes in the microbiome of 3xTg-AD mice fed with MCT or KD for 1 month.** **a** Principal Component Analysis (PCA) of each mouse microbiome according to Metacyc predicted pathways abundance obtained with PICRUST analysis. **b** Heatmap of Metacyc pathways with significant differential abundance across groups (ALDEx2 Kruskal-Wallis, adjusted  $P < 0.05$ ). **c** Heatmap of KEGG pathways with significant differential abundance across groups (ALDEx2 Kruskal-Wallis, adjusted  $P < 0.05$ ). The pathways were classified into 3 groups based on dendrogram and their abundance:

group (1) pathways enriched in 3xTg-AD mice compared to WT mice on Control diet and reduced by MCT or KD, group (2) pathways reduced or unaltered in 3xTg-AD mice compared to WT mice on Control diet and increased by MCT or KD and group (3) pathways altered in 3xTg-AD mice with no diet effect. **d** Heatmap of Pearson correlation between ASVs and predicted functional pathways of group (1). **e** Heatmap of Pearson correlation between ASVs and predicted functional pathways associated with SCFA metabolism in group (2). For **d**, **e** asterisks indicate ASVs or pathways engaged in multiple correlations.



Correlation analysis was performed between PICRUST-predicted METACYC pathways changes and ASV relative abundance to identify the ASVs involved in the predicted pathway changes. This revealed 50 ASVs significantly associated with the pathways in group (1) (Fig. 4d), 115 ASVs with pathways in group (2) (Fig. 4e, Supplementary Fig. 7a), and 91 ASVs with pathways in group (3) (Supplementary Fig. 7b). Pathways that were not

significantly associated with any ASV were removed (Supplementary Data 2). The increased relative abundances of group (1)-pathways in 3xTg-AD mice on Control diet were driven mainly by the increase of *Bifidobacterium pseudolongum*, which positively correlated with almost all these pathways including synthesis of amino acids and deoxyribonucleotides and carbohydrate degradation (Fig. 4d). Interestingly, one of the pathways that

**Fig. 5 | Increased MCT and KD-induced hippocampal spine density correlates with *Lachnospiraceae* abundance in AD mice microbiome.** **a** Average spine density in DG of 3xTg-AD mice after 5 months of dietary interventions ( $n = 6$  animals/diet, paired  $t$ -test on graph: 3xTg\_C vs 3xTg\_M, 3xTg\_C vs 3xTg\_K) Data are expressed as mean  $\pm$  SEM, red points represent mice whose gut microbiome was analyzed. **b** Spine density of dentate gyrus (DG) neurons in 3xTg-AD mice subjected to 5 months of dietary interventions and whose gut microbiome was analyzed ( $n = 15$ –36 neurons/group, Welch test on graph  $*P < 0.05$ : 3xTg\_C vs 3xTg\_M, 3xTg\_C vs 3xTg\_K). Data are expressed as median and min/max, with boxplot identifying 25–75% range. **c–e** Pearson correlation between ASV abundance in gut microbiome and spine density in DG in 3xTg-AD mice on Control or on MCT diet

( $n = 6$ ): **c** Volcano plot of correlation values highlighting significant correlation ( $P < 0.05$ ), **d** Heatmap of significant correlations (significant correlations,  $P < 0.05$  are indicated by asterisks), **e** regression plot of the most significant correlation. **f–h** Pearson correlation between ASV abundance in gut microbiome and spine density in DG in 3xTg-AD mice on Control diet or on KD ( $n = 6$ ): **f** Volcano plot of correlation values highlighting significant correlation ( $P < 0.05$ ), **g** Heatmap of significant correlations (significant correlations,  $P < 0.05$  are indicated by asterisks), **h** regression plot of the most significant correlation. **i** Dot plot of inflammatory pathways altered in the hippocampus of 3xTg-AD mice (WT\_C vs 3xTg\_C) obtained with GSEA. MCT (WT\_C vs 3xTg\_M) and KD (WT\_C vs 3xTg\_K) effects on these pathways after 6 months-intervention.

was increased in 3xTg-AD mice, L-alanine biosynthesis, correlated with the absence of multiple bacterial species (Fig. 4d). By separating the SCFA/ketone-related (Fig. 4e) from the other pathways in group (2) (Supplementary Fig. 7a), we noted that the bacterial species most increased in 3xTg-AD mice and decreased by KD and MCT, *Bifidobacterium pseudolongum*, was negatively correlated with 7/9 SCFA-related pathways stimulated by KD or MCT (Fig. 4d). This suggests that the inhibition of Bifidobacteriaceae is closely related to the metagenomic functions driven by KD or MCT. The SCFA-related pathways were also positively correlated mainly with species of Lachnospiraceae and other Firmicutes including *Peptococcaceae sp.1*, *Ruminococcaceae Paludicola sp.*, *Lachnospiraceae Lachnospiraceae. UCG.006 sp.2*, *Lachnospiraceae sp.13*, *Lachnospiraceae Blautia coccoide* (Fig. 4e). The same ASVs were also positively correlated with almost all other pathways enriched by MCT or KD (Supplementary Fig. 7a). MCT-induced isopropanol biosynthesis was highly correlated with two species of *Clostridium sensu stricto1* (Supplementary Fig. 7a, Supplementary data 2, *Clostridium sensu stricto1 sp.* Pearson correlation = 0.99, *Clostridium sensu stricto1 sp.1* Pearson correlation = 0.96). Half of the species correlating with SCFA-pathways in group (2) did not correlate with pathways in group (1) or group (3) (Supplementary Fig. 7c), suggesting the specificity of bacteria and functional changes induced by MCT and KD. Finally, *Bacteroides thetaiotaomicron* and a species of *Muribaculaceae (Muribaculaceae sp.)* were positively correlated with almost all pathways that were reduced in 3xTg-AD mice (Supplementary Fig. 7b). These species are therefore important drivers of 3xTg-AD mice microbiome phenotype unaffected by diets.

Overall, these data reveal potential functional changes associated with the increased proportion of Bifidobacteriaceae over Firmicutes families and the reduction of Bacteroidetes in the gut microbiome of 3xTg-AD mice. These changes involve macronutrient and nucleotide metabolism that were partially regulated with KD and MCT interventions, which reduce Bifidobacteriaceae processes and increase specific gut bacteria with potential effects on SCFA-related pathways and lipid metabolism.

### MCT and KD-induced changes in Lachnospiraceae abundance correlate with brain changes in AD mice

We recently demonstrated that the dietary interventions used here result in cellular and molecular changes within the brains of AD mice that are associated with improvements in learning and memory<sup>19</sup>. Since the present microbiome analyses were performed on a subset of the mice used in our previous work, we tested whether specific ASVs modulated by MCT or KD can be correlated with changes in hippocampal dendritic spine density and in line with hippocampal immune-related gene expression of 3xTg-AD mice.

MCT and KD were shown to increase dendritic spine density in the hippocampal dentate gyrus (DG) of 3xTg-AD mice after 5 months of intervention<sup>19</sup> (Fig. 5a). Similar trends were observable for the dendritic spine measurements from the subset of those mice used in the present study (Fig. 5a—red points and Fig. 5b). Using the average spine density of these mice (Fig. 5a—red points), we calculated the Pearson correlations between spine density in the DG and the relative abundance of ASVs modulated by diets in 3xTg-AD mice (Fig. 5c–h). Among 61 ASVs differentially represented in the gut microbiome of 3xTg-AD mice on Control diet versus 3xTg-AD mice on either MCT or KD (Supplementary Data 3), 7 were

associated with MCT-induced spine density increase and 8 with KD-induced spine density increase (Fig. 5c, d, f, g). These bacteria were mainly species of Lachnospiraceae positively or negatively correlated with spine density in the DG (Fig. 5d, e, g, h, Supplementary Fig. 8). Interestingly, Lachnospiraceae<sup>21,55</sup> have been implicated in the modulation of neuroinflammation and KD and MCT diets indeed regulated hippocampal-related immune gene expression. Specifically, Gene Set Enrichment Analysis (GSEA) re-analysis of our prior bulk hippocampal RNAseq data revealed down-regulation of 31 and up-regulation of 3 immune-related pathways in 3xTg-AD mice (Fig. 5i—WT\_C vs 3xTg\_C), and these were modulated toward normal by KD (Fig. 5i—WT\_C vs 3xTg\_K) and especially MCT (Fig. 5i—WT\_C vs 3xTg\_M).

Thus, MCT and KD-induced changes in Lachnospiraceae abundances are a potential contributor to the beneficial effects of these diets on the brains of AD mice.

## Discussion

This study reports the effects of MCT supplementation and the KD on the fecal microbiome in transgenic mouse models of AD.

1 month of MCT or KD intervention was sufficient to restore, respectively, 62% and 54% of disturbed ASVs in the microbiome of 3xTg-AD mice. These effects persisted after 3 months of treatment. In 5xFAD mice, MCT and KD induced specific alterations in their microbiome.

Both MCT and KD increased the alpha diversity of the microbiome in 3xTg-AD mice, whereas they either reduced or did not alter this parameter in 5xFAD mice. Both dietary interventions reduced the levels of *Bifidobacterium pseudolongum* in 3xTg-AD mice, and only KD depleted their abundance in 5xFAD mice microbiome. The abundance of *Bifidobacterium pseudolongum* was negatively correlated with ketone bodies and SCFA-related pathways. Although the link between Bifidobacteria and cognition is not clearly established, ketogenic interventions seem to reduce their levels<sup>56</sup> potentially through the production of ketone bodies. Studies reporting the anti-seizure effects of ketogenic interventions in epilepsy also reported decreased levels of Bifidobacteria after a high-fat low-carbohydrate ketogenic diet<sup>22</sup>. A small clinical trial evaluating the effect of a low-carbohydrate modified-Mediterranean ketogenic diet in MCI patients noticed a reduction in Bifidobacteria<sup>37,57</sup> in their patients, and similar observations were made in obese men treated with a low-carbohydrate ketogenic diet<sup>38</sup>. In this last study, it was proven that BHB directly inhibits the growth of different species of Bifidobacteria, which results in the decrease of pro-inflammatory immune cells in the gut and preserves the intestinal barrier<sup>38</sup>. Our study is the first to report such potential inhibitory effect of MCT supplementation on Bifidobacteria.

We observed that both diets also decreased the levels of Lactobacillaceae, especially *Lactobacillaceae HT002* and *Lactobacillaceae Johnsonii*, in 5xFAD and 3xTg-AD mice. This has been reported in other studies in humans and mice treated with low-carbohydrate ketogenic diets<sup>38,58,59</sup>. MCT and KD reduced the levels of *Escherichia coli (Shigella)* in 5xFAD mice, whereas several studies reported the opposite<sup>22,38</sup>. MCT and KD also increased the levels of several SCFA-producing bacteria, such as Lachnospiraceae<sup>60</sup> and Muribaculaceae<sup>61</sup>, in 3xTg-AD and 5xFAD mice. Further investigations are needed to understand the downstream consequences of such changes, especially in AD.

The MCT diet is an alternative ketogenic intervention using MCFA to boost ketone production<sup>11,13,14</sup> and thus avoid the energetic consequences of carbohydrate deprivation. It is interesting to observe how a small proportion of MCFA (10%) incorporated into a high-carbohydrate diet can produce similar effects on the microbiome as a low-carbohydrate, high-fat diet-like intervention (KD). However, the two interventions differed. First, mice subjected to the MCT diet did not show a permanent plasma increase in BHB. The increase in SCFA-producing bacteria can be due to the presence of transient mild ketosis, as discussed in other studies<sup>14,62,63</sup>. Second, we observed differences in the bacterial and SCFA-related pathways driven by the MCT diet compared to KD. The 3xTg-AD and 5xFAD mice on the MCT diet had reduced global levels of Lachnospiraceae compared to those on the KD. Furthermore, in 3xTg-AD mice, MCT increased the levels of specific genera of Lachnospiraceae including *Roseburia*, *Lachnoclostridium*, *Lachnospiraceae* GCA.900066575, *Marvinbryantia*, and the *Clostridium* genus *Clostridium sensu stricto*1. Some of these genera, especially *Clostridium sensu stricto*, were correlated with isopropanol biosynthesis predicted to be increased in 3xTg-AD mice on an MCT diet according to PICRUST analysis. There has been no existing study on the microbiome of AD patients treated with MCT diets. However, studies reported that high-dose of MCT supplementation in mice on a standard diet resulted in increased levels of Lachnospiraceae<sup>64</sup>. A high-fat MCT, low-carbohydrate diet in a Parkinson's disease mouse model increased some species of Lachnospiraceae and *Clostridia*<sup>65</sup> with no indication about the genus.

*Clostridium* species catalyze isopropanol biosynthesis from pyruvate, which is first metabolized into acetone and then isopropanol<sup>53,66</sup>. This suggests that the MCT diet promotes the production of isopropanol instead of the production of lactate from pyruvate, which would have been observed in a normal carbohydrate-enriched diet. Further investigations are required to understand the function of this reaction and the benefits in the context of AD.

We have shown that 4 months old 3xTg-AD mice on a standard diet presented alterations in the microbiome, which tended to decrease with aging. These mice had lower microbiome diversity, a distinct microbiome composition compared to age-matched WT mice, and altered relative abundance of 102 ASVs at 4 months of age. Among these ASVs, we have reported increased levels of *Bifidobacterium pseudolongum* and reduced levels of *Bacteroidota*, resulting in a higher F/B ratio, and altered abundance in several families of Firmicutes. In 3 months old 5xFAD mice, we observed minor differences compared to WT mice, which mainly disappeared at 5 months of age. Young 5xFAD mice microbiome was characterized by enriched levels of *Escherichia coli* (*Shigella*), *Muribaculaceae*, and *Enterococcaceae* *Enterococcus*, as well as decreased levels of *Deftuivittaleaceae* *UCC 011 sp.*, *Peptostreptococcaceae* *Romboutsia ilealis*.1, *Eggerthellaceae* *Parvibacter*, and altered levels of two species of *Lachnospiraceae*.

Similar to our observations, early changes in the microbiome of 3xTg-AD mice were shown to resorb over time in a longitudinal study from 4 to 13 months of age<sup>33</sup>. Changes in the gut microbiome in people at a high risk of developing AD dementia have been analyzed by few studies. Cognitively normal individuals with cerebral amyloid beta deposition presented minor alterations and no differences in alpha or beta diversity compared with those with no amyloid deposition<sup>67</sup>, similar to what was observed in our 5xFAD mice. Other studies reported changes in individuals with mild cognitive impairment (MCI) such as lower levels of *Bacteroidetes*<sup>25,68,69</sup>, higher levels of *Escherichia*<sup>68</sup>, *Enterobacteriaceae*<sup>25</sup>, *Bifidobacterium*<sup>68</sup>, *Lachnospiraceae* *Roseburia*<sup>68,69</sup>, and *Lactobacillus* (*Lactobacillaceae*)<sup>68</sup>, as observed in the present study. A lower alpha diversity associated with reduced Firmicutes and increased *Bacteroidetes* was also reported in individuals with subjective cognitive decline and MCI<sup>70</sup>. In symptomatic AD individuals, the existing studies reported lower alpha-diversity and clear distinct microbiome alterations with the most consistent changes being reduced Firmicutes<sup>24,71,72</sup> especially Lachnospiraceae<sup>32,73-75</sup> and Clostridiaceae families, reduced *Bacteroidota*<sup>27,71,73,76</sup> and increased *Escherichia coli*<sup>27,71,72</sup>. Interestingly *Bifidobacterium* levels were reported either increased or decreased in AD or MCI patients<sup>23,24,26,32,68,73,75</sup>. Genotypes of *Bifidobacterium* are often considered beneficial for gut health and are used in probiotic cocktails<sup>54</sup>. Here,

we highlight the fact that these bacteria are increased by genetic risk factors for AD; therefore, more research is needed to understand their role in AD.

The predicted functional changes based on alterations in the microbiome of 3xTg-AD mice suggest impaired metabolic processes of macro-nutrients. *Bifidobacterium pseudolongum* and *Lactobacillaceae* HT002 were associated with increased L-aspartate, L-threonine, L-lysine, and L-methionine biosynthetic pathways, sucrose degradation, hexose and xylose fermentation to pyruvate/lactate, and deoxyribonucleotide synthesis. Reduced levels of *Bacteroidota*, especially *Bacteroides thetaiotaomicron* and *Muribaculaceae*, correlated with a decrease in the degradation of mannan, inositol, chondroitin sulfate, and 4-deoxy-L-threo-hex-4-enopyranuronate. Some of these correlations have been proven in the literature<sup>54,77</sup>, for instance, the degrading effect of *Bacteroides thetaiotaomicron* on chondroitin sulfate<sup>77</sup>.

Some altered pathways observed in this study have been described in the brain, body or gut microbiome in the context of AD. For instance, higher microbial abundance of the sucrose degradation (sucrose phosphorylase) and s-adenosyl-methionine (SAME) cycle 1 pathways has also been reported in MCI patients when compared to demented ones<sup>76</sup>. The 4-deoxy-L-threo-hex-4-enopyranuronate degradation<sup>53</sup> another sugar catabolic pathway downstream of chondroitin sulfate degradation<sup>53</sup> and implicated in SCFA production<sup>77,78</sup> was also disturbed in AD and MCI<sup>72,79</sup>. Chondroitin sulfate derived proteoglycans play a role in the response to neurological damages and might be involved in AD<sup>80</sup>. Nevertheless, little is known about the microbial chondroitin sulfate. Methionine levels and molecules involved in its cycle, such as homocysteine, have also been documented in patients with AD and MCI, as well as in interventions targeting this compound<sup>81-83</sup>. For instance, a genetic model of methionine restriction in drosophila highlighted the importance of microbiota-derived methionine in aging<sup>83</sup>.

In addition, our results also support the idea that the AD microbiome is characterized by a shift from SCFA-producing bacteria (*Bacteroidetes*, *Lachnospiraceae*) toward lactate-producing bacteria (*Bifidobacterium*, *Lactobacillaceae*)<sup>32,75,84,85</sup>. Reduced fecal levels of SCFA along different stages of AD<sup>86,87</sup> have been reported. Notably, a study in APP/PS1 mice described excessive levels of lactic acid and reduced levels of SCFAs in their fecal matter<sup>88</sup>.

Altogether, the onset of microbial alterations during early or pre-symptomatic stages of AD suggests a contribution of microbial species to AD pathophysiology through alterations in sugar, lactate, SCFA, and amino acids.

Both 3xTg-AD and 5xFAD mice showed reduced upregulation of BHB, increased F/B ratio and higher body weight gain under the KD compared to WT mice on the same diet. In the case of 5xFAD mice fed the KD, the microbiome composition was distinct from that of their WT littermates, while this difference was not present in the Control diet. Furthermore, 5xFAD mice on the MCT diet showed reduced alpha diversity due to reduced levels of Firmicutes (Lachnospiraceae, Oscillospiraceae, Lactobacillaceae, Ruminococcaceae). Together, these responses demonstrate beneficial effects of these interventions on the brain can be accompanied by unexpected peripheral and microbiome changes. The specific metabolic response of AD mice to KD suggests latent metabolic defects related to AD pathophysiology which need to be considered when designing such dietary intervention in AD patients.

A first limitation of this study is the sample size 3 or 4 per group, which if increased may reduce variability within the groups. Second, the lack of information regarding the levels of microbial metabolites limits the complete interpretation of microbiome alterations, as changes in the relative abundance of bacteria do not necessarily involve changes in metabolites. Similarly, 16S rRNA sequencing limits the interpretation of functional changes. A metatranscriptomic or metagenomic analysis would give more indication about the presence of the species, but also about their activity levels through the transcripts.

In conclusion, this study reinforces the idea of microbial alterations existing in the early stages of AD. This suggests that genetic predispositions

to AD induce a microbial shift toward lactate-producing bacteria and impaired metabolic processing of macronutrients. These alterations can be prevented by MCT supplementation or KD, which increase the levels of SCFA-producing bacteria and decrease those of the main lactate-producing bacteria. However, ketogenic strategies drive different bacterial genera and different mechanisms, which require further investigation. This study proposes that the microbiome might contribute to AD pathophysiology and represent a therapeutic target of ketogenic interventions.

## Materials and methods

### Mice and treatment

**5xFAD mice.** The generation and characterization of the model were previously described<sup>43,89</sup>. The 5xFAD (Jackson laboratory MMRC stock#: 34840-JAX) transgenic mouse model carries five familial Alzheimer's disease (FAD) mutations, including *Swedish* (K670N, M671L), *Florida* (I716V), and *London* (V717I) mutations in the APP transgene, as well as *M146L* and *L286V* FAD mutations in the PSEN1 transgene, both under mouse Thy1 promoter. These transgenic mice were bred onto the B6SJLF1/J background (Jackson laboratory stock#: 100012). For our experiments in this study, we utilized both heterozygous mutant mice and non-carrier mice as appropriate controls.

**3xTg-AD mice and B6;129 genotype wild type.** The generation and characterization of the model were previously described<sup>41,90</sup>. 3xTg-AD mice (Jackson laboratory MMRC stock#: 34830-JAX) possess three human dementia-causing mutations that lead to AD's pathological traits: **APP<sub>Swe</sub>** and **tau<sub>P301L</sub>** encoded in two independent transgene constructs under control of the central nervous system (CNS) mouse regulatory element Thy1.2, co-microinjected into single-cell embryos harvested from homozygous mutant **PS1<sub>M146V</sub>** knock in (PS1-KI) mice. Wild type mice are B6;129 (WT, the 3xTg-AD background genotype, Jackson laboratory stock#: 101045) obtained from a cross between C57BL/6J females (B6) and 129S1/SvImJ males (129S).

**Housing and dietary interventions.** Mice received either a Control diet (C, 70% carbohydrate, 20% long-chain triglycerides, 10% protein, 4.1 kcal/g, Research Diets product #D17121209I), a Control diet enriched with medium-chain triglycerides (MCT, 70% carbohydrate, 10% long-chain triglycerides, 10% medium-chain triglycerides (Caprylic acid to Capric acid ratio of 3:2), 10% protein, 4.1 kcal/g, Research Diets product #D17121210I) or a carbohydrate-free ketogenic-like diet (KD, 90% long-chain triglycerides, 10% protein, 6.7 kcal/g, Research Diets product# : D10070801). All diets contain 50 g of fibers in the form of cellulose. See table - detailed composition.

All animals were group-housed (3–4 per cage) in reverse cycle room (12 h Dark-light cycle 10AM—OFF, 10PM—ON) with food/water ad libitum. 5xFAD mice were on diets for 3 months, spanning ages 2–5 months. 3xTg-AD mice were on diets for 5 months, spanning ages 3–8 months to analyze protective changes at pre-symptomatic level.

### Metabolic features

**Body weight monitoring.** The food pellets were changed twice a week according to the food company recommendations. The mice were weighed 28 days before the beginning of the experiment and twice from day 0 to day 28. From this date until day 140, mice were weighted once or twice a month.

**Beta-hydroxybutyrate and glucose monitoring.** At different time points (Day 0, Day 14, Day 85, Day 140) circulating beta-hydroxybutyrate (BHB) levels were measured using the freestyle precision neo (Abbott, product#: ART30531) with the blood BHB test strips (Abbott, REF#: 70748-75). Glycemia was monitored using a blood glucose monitoring system (Abbott, ART20771) with the reading strips (Abbott, 70825-70). The mice were pricked in the tail vein with a needle to have the required blood drops for the strips.

### Sample collection

Fecal matters were collected from each mouse at different timepoints of dietary interventions: Day 28, Day 85 and Day 140 (only 3xTg-AD mice) on diet. For 3xTg-AD mice, this corresponded to 4 months old, 6 months old and 8 months old. For 5xFAD mice, it was at 3 months old and 5 months old.

### DNA library preparation and 16S rRNA sequencing

16S amplicon libraries were prepared according to our previous works<sup>91,92</sup> by a blinded experimenter. Extractions of microbial DNA from the stool samples were performed using the QIAamp DNA stool mini kit (Qiagen) with some modifications<sup>93–95</sup>. Briefly, stool sample is resuspended in 500 µl of ASL Buffer (Qiagen) with 250 µl of 0.1 mm glass beads. Samples were homogenized for 3 min at 6500 rpm (Precellys 24), then incubated at 95 °C for 15 min. Another round of homogenization was performed for 3 min at 6500 rpm and then centrifuged for 10 min at 13 000 rpm at room temperature. The supernatants were transferred to 1 ml of 100% EtOH and 10 µl 3 M sodium acetate (pH = 5.2), then precipitated at –80 °C for 15 min. Samples were centrifuged at 4 °C for 20 min at 13,000 rpm and pellets were resuspended in 200 µl Tris 10 mM pH = 7.5 and EDTA 1 mM. 2 µl for DNase-Free RNase A (10 mg/mL) was added and incubated at 37 °C for 30 min followed by the addition of 15 µl of proteinase K and 200 µl of AL Buffer (Qiagen) incubated at 70 °C for 30 min. 200 µl of 100% EtOH was added and transferred to a QIAamp column. The next step was done according to the manufacturer's instructions and the DNA samples were stored at –80°C. For the amplification of the V4 region of the bacterial 16S rRNA gene, the 515F (5'-GTGCCAGCMGCCGCGGTAA-3') and 806 R (5'-GGACTACHVGGGTWTCTAAT-3') paired primers were used with 5 ng of microbial genomic DNA<sup>96</sup>. Lastly, the pooled and indexed libraries (60 ng) were sequenced in paired-end modus on an Illumina MiSeq<sup>97</sup> at the RNomics Platform of the University of Sherbrooke (<https://rnomics.med.usherbrooke.ca/>).

### Bioinformatics analysis

Quality control, filtering and trimming (truncate R1 and R2 reads after 240 and 160 bp, respectively; after truncation, sequences with more than 0 Ns and with higher than 2 “expected errors” were discarded; truncate reads at the first instance of a quality score less than or equal to 2) of fastq files, evaluation of error rate of amplicons, merging of paired reads, amplicon sequence variant table (ASV) table construction, chimera removal, taxonomy assigning (through SILVA database “silva nr99 v138.1 wSpecies train set.fa.gz”) were all performed with R package DADA2 v1.24.0<sup>98</sup>. The selected ASV were present in at least 10 samples and had depth sequencing of at least 1000 reads.

The overall structure of datasets and individual phenotypic characteristics were explored through multidimensional analysis plots such as heatmap and multidimensional scaling (MDS) plots utilizing R package metagenomeSeq v1.38.0<sup>99,100</sup>. The first 3 most important MDS axes were 3D visualized through R package plotly v4.11.0. Within-habitat diversity species richness (Alpha diversity) analysis was performed through R package phyloseq v1.30.0<sup>101</sup> utilizing Shannon, Simpson and Chao1 indices. Mean comparisons were tested through R package ggpubr v0.6.0 and included non-parametric Wilcoxon test for two-group comparison and non-parametric Kruskal-Wallis test for multiple groups comparisons. Variance in the structure of the population (Beta diversity) with Bray-Curtis metric was also performed with phyloseq v1.30.0. Here to test if the groups were significantly different from each other we performed a Permanova test using the adonis function from the vegan v2.6-4 R package. To track the longitudinal microbiome changes, more specifically to check how beta diversity changed across diet time, we created volatility plots through QIIME2<sup>102</sup> using Unweighted Unifrac and Jaccard metrics.

Next, we performed a differential expression analysis to statistically compare previously obtained ASVs among the different pre-determined groups (WT C vs 3xTg C, WT C vs 3xTg M, WT C vs 3xTg KD). First, due to varying depths of coverage across mice, we needed to normalize data. To reduce biases resulting from preferentially sampled taxa we normalized by

using CSS (Cumulative-Sum Scaling)<sup>103</sup> implemented in metagenomeSeq<sup>99</sup>. We sampled same mice between different conditions, so their duplicated effect cannot be omitted from the successive statistical analysis, however differences between mice were not of direct interest; to account for all of this we decided to treat mice IDs as random effect in a mixed effects model where our fixed effects were just reduced to our group of interest<sup>104</sup>. Thus, mice IDs were considered as a blocking variable. Their apport was calculated through the function duplicateCorrelation of R package limma v3.50.1<sup>105</sup> and included in the subsequent fitted model. All interesting contrasts (WT C vs 3xTg C, WT C vs 3xTg M, WT C vs 3xTg KD) were then statistically evaluated and visualized (through volcano plots) with limma where differential expressed ASVs were filtered at a P-adjusted threshold value at 0.05. Heatmaps were also used to visualize the diet effect on microbial alterations of AD mice. They were generated with R package Pretty Heatmaps (Raivo Kolde (2019). pheatmap: Pretty Heatmaps. R package version 1.0.12. <https://CRAN.R-project.org/package=pheatmap>).

Venn diagrams were created to better visualize common differentially expressed ASVs among conditions of interest. The same was done for 5xFAD mice following the interesting contrasts (WT C vs 5xFAD C, WT C vs 5xFAD M, WT C vs 5xFAD KD, WT C vs WT M, 5xFAD C vs 5xFAD M, WT C vs WT KD, 5xFAD C vs 5xFAD KD).

To predict functional abundances based on marker gene sequences we used PICRUSt2<sup>106</sup>. We then performed DA analysis, using ALDEx2 Kruskal-Wallis test, on its abundance data outputs, annotated under Metacyc and KEGG consortia, with R package ggpicrust2 v1.7.330<sup>107</sup>. We filter out those pathways that did not passed a P adjusted of 0.05. Using resulting differentially expressed pathways we plotted a heatmap (R package Pretty Heatmaps) and barplots with error bars (to limit the results to better visualize the plot, here we ordered by decrescent adjusted P and selected just the top 20). Metacyc pathway PCA was performed with R package factoextra v1.0.7 and visualized with ggplot R package.

### Statistical analysis and reproducibility

The sample sizes were calculated to reach a degree of freedom of ANOVA between 10 and 18<sup>108</sup> and mice were randomly assigned to experimental groups, ensuring that each litter was distributed across groups :

#### Day 28 on diet

Control diet: WT  $n = 4$ , 3xTg-AD  $n = 4$  / WT  $n = 4$ , 5xFAD  $n = 4$

MCT diet: WT  $n = 4$ , 3xTg-AD  $n = 4$  / WT  $n = 4$ , 5xFAD  $n = 4$

KD: WT  $n = 4$ , 3xTg-AD  $n = 4$  / WT  $n = 4$ , 5xFAD  $n = 4$

#### Day 85 on diet

Control diet: WT  $n = 4$ , 3xTg-AD  $n = 4$  / WT  $n = 4$ , 5xFAD  $n = 4$

MCT diet: WT  $n = 4$ , 3xTg-AD  $n = 4$  / WT  $n = 4$ , 5xFAD  $n = 4$

KD: WT  $n = 4$ , 3xTg-AD  $n = 4$  / WT  $n = 4$ , 5xFAD  $n = 4$

#### Day 140 on diet

Control diet: WT  $n = 1$  (due to technical issues, the amplification did not work for 2 animals), 3xTg-AD  $n = 4$

MCT diet: WT  $n = 3$ , 3xTg-AD  $n = 3$

KD: WT  $n = 3$ , 3xTg-AD  $n = 3$

The correlation between varying ASVs and predicted functional changes was calculated in R using Pearson method. We filtered out the correlation that did not passed an adjusted  $P$  of 0.05 (Benjamini and Hochberg's method) and visualized with ggplot heatmap. The correlation between ASVs and hippocampal spine density was calculated using Pearson method ( $P < 0.05$ ). Statistical tests for metabolic monitoring and relative abundance levels at phylum and family levels were performed using GraphPad Prism v10.0 (GraphPad Software). Mixed effect analysis and two-way ANOVA with Sidak post hoc test were used for appropriate situations. The pair-wise comparison tests were performed only for the following contrasts : for genotype effect within the same diet/ WT C vs 3xTg C, WT M vs 3xTg M, WT KD vs 3xTg KD, for diet effect within the same genotype / WT C vs WT M, WT C vs WT KD, 3xTg C vs 3xTg M, 3xTg C vs 3xTg KD. Data are presented as means  $\pm$  standard errors of the mean or median with minimum and maximum. Statistical tests performed are detailed in the

legend for each figure.  $P < 0.05$  was considered statistically significant and  $0.05 < P < 0.1$  was considered nearly significant.

### Nomenclature

A specific bacterium is named based on its genus and species (ex: *Bifidobacterium pseudolongum*). When the specific genus or the species is not known, the bacterium is named with the most precise taxonomical group plus "sp." in the text or "NA" on the graphs (ex: *Muribaculaceae sp.*, *Muribaculaceae\_NA\_NA*).

### Gene set enrichment analysis on hippocampus transcriptome

GSEA was performed using the "gseGO" function from the clusterProfiler package in R software v4.5.0 within the RStudio development environment v2025.05.0. Gene lists for each comparison were first ranked based on the formula:  $-\log_{10}(P\text{-value}) \times \text{sign}(\text{Fold Change})$ . The "Biological Process (BP)" ontology was specified, and the genome wide annotation for mouse (org.Mm.eg.db) was used as the reference. Pathways with a gene set size between 5 and 600 were included, and those with a false discovery rate (FDR)  $q < 0.05$ , adjusted by the Benjamini-Hochberg method for multiple comparisons, were considered significant. Among the enriched pathways, those related to immune response and inflammation were specifically identified through manual curation.

### Ethics

All experiments were carried out in accordance with the guidelines of the Canadian Council of Animal Care and were approved by the Institutional Animal Care Committee of the University of Sherbrooke (protocol #2020-2688).

### Reporting summary

Further information on research design is available in the Nature Portfolio Reporting Summary linked to this article.

### Data availability

The data underlying this article are available in the article, in its online supplementary material and supplementary datasets. Sequencing data are available on Sequence Read Archive (SRA): PRJNA1160852.

### Code availability

The source codes used to generate these results are based on resources referenced in the method section of the present article and are available upon request to the corresponding authors.

Received: 13 February 2025; Accepted: 3 November 2025;

Published online: 07 December 2025

### References

1. Mosconi, L. et al. Early detection of Alzheimer's disease using neuroimaging. *Exp. Gerontol.* **42**, 129–138 (2007).
2. Association, A. S. 2021 Alzheimer's disease facts and figures. *Alzheimer's Dement.* **17**, 327–406 (2021).
3. Arnold, S. E. et al. Brain insulin resistance in type 2 diabetes and Alzheimer disease: concepts and conundrums. *Nat. Rev. Neurol.* **14**, 168–181 (2018).
4. Livingston, G. et al. Dementia prevention, intervention, and care: 2020 report of the *Lancet* Commission. *Lancet* **396**, 413–446 (2020).
5. Scheltens, P. et al. Alzheimer's disease. *Lancet* **397**, 1577–1590 (2021).
6. Trushina, E. Alzheimer's disease mechanisms in peripheral cells: promises and challenges. *Alzheimer's Dement. (N. Y.)* **5**, 652–660 (2019).
7. Fortier, M. et al. A ketogenic drink improves cognition in mild cognitive impairment: results of a 6-month RCT. *Alzheimer's Dement.* <https://doi.org/10.1002/alz.12206> (2020).

8. Phillips, M. C. L. et al. Randomized crossover trial of a modified ketogenic diet in Alzheimer's disease. *Alzheimer's Res. Ther.* **13**, 51 (2021).
9. Cunnane, S. C. et al. Brain energy rescue: an emerging therapeutic concept for neurodegenerative disorders of ageing. *Nat. Rev. Drug Discov.* **19**, 609–633 (2020).
10. Newman, J. C. & Verdin, E.  $\beta$ -hydroxybutyrate: a signaling metabolite. *Annu Rev. Nutr.* **37**, 51–76 (2017).
11. Augustin, K. et al. Mechanisms of action for the medium-chain triglyceride ketogenic diet in neurological and metabolic disorders. *Lancet Neurol.* **17**, 84–93 (2018).
12. Vandenberghe, C. et al. Medium chain triglycerides modulate the ketogenic effect of a metabolic switch. *Front. Nutr.* **7**, <https://doi.org/10.3389/fnut.2020.00003> (2020).
13. Lin, T. Y., Liu, H. W. & Hung, T. M. The ketogenic effect of medium-chain triacylglycerides. *Front Nutr.* **8**, 747284 (2021).
14. St-Pierre, V. et al. Plasma ketone and medium chain fatty acid response in humans consuming different medium chain triglycerides during a metabolic study day. *Front. Nutr.* **6**, <https://doi.org/10.3389/fnut.2019.00046> (2019).
15. Fortier, M. et al. A ketogenic drink improves brain energy and some measures of cognition in mild cognitive impairment. *Alzheimer's Dement.* **15**, 625–634 (2019).
16. Bohnen, J. L. B., Albin, R. L. & Bohnen, N. I. Ketogenic interventions in mild cognitive impairment, Alzheimer's disease, and Parkinson's disease: a systematic review and critical appraisal. *Front. Neurol.* **14**, <https://doi.org/10.3389/fneur.2023.1123290> (2023).
17. Croteau, E. et al. Ketogenic medium chain triglycerides increase brain energy metabolism in Alzheimer's disease. *J. Alzheimer's Dis.* **64**, 551–561 (2018).
18. Krolak-Salmon, P. et al. Efficacy and safety of exogenous ketones in people with mild neurocognitive disorder and Alzheimer's disease: a systematic literature review. *Nutr. Rev.* **83**, e1034–e1048 (2025).
19. M'Bra, P. E. H. et al. Medium-chain triglycerides improve cognition and systemic metabolism in mouse models of Alzheimer's disease. *Brain*. <https://doi.org/10.1093/brain/awaf267> (2025).
20. Cryan, J. F., O'Riordan, K. J., Sandhu, K., Peterson, V. & Dinan, T. G. The gut microbiome in neurological disorders. *Lancet Neurol.* **19**, 179–194 (2020).
21. Bairamian, D. et al. Microbiota in neuroinflammation and synaptic dysfunction: a focus on Alzheimer's disease. *Mol. Neurodegener.* **17**, 19 (2022).
22. Mazandarani, M., Lashkarbolouk, N., Ejtahed, H.-S. & Qorbani, M. Does the ketogenic diet improve neurological disorders by influencing gut microbiota? A systematic review. *Nutr. J.* **22**, 61 (2023).
23. Khedr, E. M., Omeran, N., Karam-Allah Ramadan, H., Ahmed, G. K. & Abdelwarith, A. M. Alteration of gut microbiota in Alzheimer's disease and their relation to the cognitive impairment. *J. Alzheimers Dis.* **88**, 1103–1114 (2022).
24. Vogt, N. M. et al. Gut microbiome alterations in Alzheimer's disease. *Sci. Rep.* **7**, 13537 (2017).
25. Liu, P. et al. Altered microbiomes distinguish Alzheimer's disease from amnesic mild cognitive impairment and health in a Chinese cohort. *Brain Behav. Immun.* **80**, 633–643 (2019).
26. Lopizzo, N. et al. Identification of gut microbiota signature in Alzheimer's disease: possible role in influencing peripheral inflammation. *Eur. Neuropsychopharmacol.* **29**, S167–S168 (2019).
27. Cattaneo, A. et al. Association of brain amyloidosis with pro-inflammatory gut bacterial taxa and peripheral inflammation markers in cognitively impaired elderly. *Neurobiol. Aging* **49**, 60–68 (2017).
28. Zhang, T., Gao, G., Kwok, L.-Y. & Sun, Z. Gut microbiome-targeted therapies for Alzheimer's disease. *Gut Microbes* **15**, 2271613 (2023).
29. Du, Y. et al. The role of short chain fatty acids in inflammation and body health. *Int. J. Mol. Sci.* **25**, 7379 (2024).
30. Kimura, I. et al. Short-chain fatty acids and ketones directly regulate sympathetic nervous system via G protein-coupled receptor 41 (GPR41). *Proc. Natl Acad. Sci.* **108**, 8030–8035 (2011).
31. Fusco, W. et al. Short-chain fatty-acid-producing bacteria: key components of the human gut microbiota. *Nutrients* **15**, <https://doi.org/10.3390/nu15092211> (2023).
32. Ling, Z. et al. Structural and functional dysbiosis of fecal microbiota in chinese patients with Alzheimer's disease. *Front. Cell Dev. Biol.* **8**, <https://doi.org/10.3389/fcell.2020.634069> (2021).
33. Borsom, E. M. et al. Predicting neurodegenerative disease using prepathology gut microbiota composition: a longitudinal study in mice modeling Alzheimer's disease pathologies. *Microbiol. Spectr.* **11**, e03458–03422 (2023).
34. Chen, C. et al. Gut dysbiosis contributes to amyloid pathology, associated with C/EBP $\beta$ /AEP signaling activation in Alzheimer's disease mouse model. *Sci. Adv.* **6**, eaba0466 (2020).
35. Rew, L., Harris, M. D. & Goldie, J. The ketogenic diet: its impact on human gut microbiota and potential consequent health outcomes: a systematic literature review. *Gastroenterol. Hepatol. Bed Bench* **15**, 326–342 (2022).
36. Rivière, A., Selak, M., Lantin, D., Leroy, F. & De Vuyst, L. Bifidobacteria and butyrate-producing colon bacteria: importance and strategies for their stimulation in the human gut. *Front Microbiol* **7**, 979 (2016).
37. Nagpal, R., Neth, B. J., Wang, S., Craft, S. & Yadav, H. Modified Mediterranean-ketogenic diet modulates gut microbiome and short-chain fatty acids in association with Alzheimer's disease markers in subjects with mild cognitive impairment. *EBioMedicine* **47**, 529–542 (2019).
38. Ang, Q. Y. et al. Ketogenic diets alter the gut microbiome resulting in decreased intestinal Th17 cells. *Cell* **181**, 1263–1275.e1216 (2020).
39. Gong, X. et al. Gut flora and metabolism are altered in epilepsy and partially restored after ketogenic diets. *Micro. Pathog.* **155**, 104899 (2021).
40. Dunham, S. J. B. et al. Longitudinal analysis of the microbiome and metabolome in the 5xfAD mouse model of Alzheimer's disease. *mBio* **13**, e01794–01722 (2022).
41. Oddo, S. et al. Triple-transgenic model of Alzheimer's disease with plaques and tangles: intracellular Abeta and synaptic dysfunction. *Neuron* **39**, 409–421 (2003).
42. Javonillo, D. I. et al. Systematic phenotyping and characterization of the 3xTg-AD mouse model of Alzheimer's disease. *Front. Neurosci.* **15**, <https://doi.org/10.3389/fnins.2021.785276> (2022).
43. Oblak, A. L. et al. Comprehensive evaluation of the 5XFAD mouse model for preclinical testing applications: a MODEL-AD study. *Front Aging Neurosci.* **13**, 713726 (2021).
44. Robison, L. S. et al. Sex differences in metabolic phenotype and hypothalamic inflammation in the 3xTg-AD mouse model of Alzheimer's disease. *Biol. Sex. Differ.* **14**, 51 (2023).
45. Peeters, J. et al. Exploring the Microbiome Analysis and Visualization Landscape. *Frontiers in Bioinformatics* **1**, <https://doi.org/10.3389/fbinf.2021.774631> (2021).
46. Wang, Y. et al. Protective effect of zinc gluconate on intestinal mucosal barrier injury in antibiotics and LPS-induced mice. *Front. Microbiol.* **15**, <https://doi.org/10.3389/fmicb.2024.1407091> (2024).
47. Blik Tijds, F. V. D. K., Marc Galland. *RNA-seq lesson*, <<https://github.com/ScienceParkStudyGroup/maseq-lesson>>.
48. Chen, J. et al. Associating microbiome composition with environmental covariates using generalized UniFrac distances. *Bioinformatics* **28**, 2106–2113 (2012).
49. Ley, R. E. et al. Obesity alters gut microbial ecology. *Proc. Natl. Acad. Sci.* **102**, 11070–11075 (2005).
50. Koliada, A. et al. Association between body mass index and Firmicutes/Bacteroidetes ratio in an adult Ukrainian population. *BMC Microbiol* **17**, 120 (2017).

51. Cheng, Z., Zhang, L., Yang, L. & Chu, H. The critical role of gut microbiota in obesity. *Front. Endocrinol.* **13**, 1025706 (2022).
52. Smith, E. & Morowitz, H. J. Universality in intermediary metabolism. *Proc. Natl Acad. Sci.* **101**, 13168–13173 (2004).
53. Caspi, R. et al. The MetaCyc database of metabolic pathways and enzymes—a 2019 update. *Nucleic Acids Res* **48**, D445–d453 (2020).
54. O’Callaghan, A. & van Sinderen, D. Bifidobacteria and their role as members of the human gut microbiota. *Front. Microbiol.* **7**, <https://doi.org/10.3389/fmicb.2016.00925> (2016).
55. Bostick, J. W., Schonhoff, A. M. & Mazmanian, S. K. Gut microbiome-mediated regulation of neuroinflammation. *Curr. Opin. Immunol.* **76**, 102177 (2022).
56. Ross, F. C. et al. The interplay between diet and the gut microbiome: implications for health and disease. *Nat. Rev. Microbiol.* **22**, 671–686 (2024).
57. Ayten, Ş. & Bilici, S. Modulation of gut microbiota through dietary intervention in neuroinflammation and Alzheimer’s and Parkinson’s diseases. *Curr. Nutr. Rep.* **13**, 82–96 (2024).
58. Dilimulati, D. et al. Ketogenic diet modulates neuroinflammation via metabolites from *Lactobacillus reuteri* after repetitive mild traumatic brain injury in adolescent mice. *Cell. Mol. Neurobiol.* **43**, 907–923 (2023).
59. Klein, M. S. et al. Metabolomic modeling to monitor host responsiveness to gut microbiota manipulation in the BTBRT+tf/j mouse. *J. Proteome Res.* **15**, 1143–1150 (2016).
60. Vacca, M. et al. The controversial role of human gut lachnospiraceae. *Microorganisms* **8**, <https://doi.org/10.3390/microorganisms8040573> (2020).
61. You, H. et al. The therapeutic effect of SCFA-mediated regulation of the intestinal environment on obesity. *Front. Nutr.* **9**, <https://doi.org/10.3389/fnut.2022.886902> (2022).
62. Shcherbakova, K. et al. Short- and long-term cognitive and metabolic effects of medium-chain triglyceride supplementation in rats. *Heliyon* **9**, e13446 (2023).
63. Ota, M. et al. Effects of a medium-chain triglyceride-based ketogenic formula on cognitive function in patients with mild-to-moderate Alzheimer’s disease. *Neurosci. Lett.* **690**, 232–236 (2019).
64. Zhang, J. et al. Dietary additive octyl and decyl glycerate modulates metabolism and inflammation under different dietary patterns with the contribution of the gut microbiota. *Food Funct.* **14**, 525–540 (2023).
65. Zhang, W. et al. Neuroprotective effect of a medium-chain triglyceride ketogenic diet on MPTP-induced Parkinson’s disease mice: a combination of transcriptomics and metabolomics in the substantia nigra and fecal microbiome. *Cell Death Discov.* **9**, 251 (2023).
66. Zhou, J. et al. An acetate-independent pathway for isopropanol production via HMG-CoA in *Escherichia coli*. *J. Biotechnol.* **359**, 29–34 (2022).
67. Jung, J. H. et al. Gut microbiome alterations in preclinical Alzheimer’s disease. *PLoS ONE* **17**, e0278276 (2022).
68. Li, B. et al. Mild cognitive impairment has similar alterations as Alzheimer’s disease in gut microbiota. *Alzheimer’s Dement.* **15**, 1357–1366 (2019).
69. Yu, B. et al. Disruptions of gut microbiota are associated with cognitive deficit of preclinical Alzheimer’s disease: a cross-sectional study. *Curr. Alzheimer Res.* <https://doi.org/10.2174/0115672050303878240319054149> (2024).
70. Chen, G., Zhou, X., Zhu, Y., Shi, W. & Kong, L. Gut microbiome characteristics in subjective cognitive decline, mild cognitive impairment and Alzheimer’s disease: a systematic review and meta-analysis. *Eur. J. Neurol.* **30**, 3568–3580 (2023).
71. Bonnechère, B., Amin, N. & van Duijn, C. What are the key gut microbiota involved in neurological diseases? A systematic review. *Int. J. Mol. Sci.* **23**, 13665 (2022).
72. Fabi, J. P. The connection between gut microbiota and its metabolites with neurodegenerative diseases in humans. *Metab. Brain Dis.* **39**, 967–984 (2024).
73. Zhuang, Z.-Q. et al. Gut microbiota is altered in patients with Alzheimer’s disease. *J. Alzheimer’s Dis.* **63**, 1337–1346 (2018).
74. Haran J., P. et al. Alzheimer’s disease microbiome is associated with dysregulation of the anti-inflammatory P-glycoprotein pathway. *mBio* **10**, <https://doi.org/10.1128/mbio.00632-00619> (2019).
75. Chen, L. et al. A comparison of the composition and functions of the oral and gut microbiotas in Alzheimer’s patients. *Front. Cell. Infect. Microbiol.* **12**, 942460 (2022).
76. Jeong, S. et al. Cognitive function associated with gut microbial abundance in sucrose and S-adenosyl-L-methionine (S-AMe) metabolic pathways. *J. Alzheimer’s Dis.* **87**, 1115–1130 (2022).
77. Wang, Y., Ma, M., Dai, W., Shang, Q. & Yu, G. *Bacteroides salyersiae* is a potent chondroitin sulfate-degrading species in the human gut microbiota. *Microbiome* **12**, 41 (2024).
78. He, K., Liu, M., Wang, Q., Chen, S. & Guo, X. Combined analysis of 16S rDNA sequencing and metabolomics to find biomarkers of drug-induced liver injury. *Sci. Rep.* **13**, 15138 (2023).
79. Luo, Y.-X., Yang, L.-L. & Yao, X.-Q. Gut microbiota-host lipid crosstalk in Alzheimer’s disease: implications for disease progression and therapeutics. *Mol. Neurodegener.* **19**, 35 (2024).
80. Lin, J. -z, Duan, M. -r, Lin, N. & Zhao, W. -j The emerging role of the chondroitin sulfate proteoglycan family in neurodegenerative diseases. *Rev. Neurosci.* **32**, 737–750 (2021).
81. Zhao, Y. et al. Effects of S-adenosylmethionine on cognition in animals and humans: a systematic review and meta-analysis of randomized controlled trials. *J. Alzheimers Dis.* **94**, S267–s287 (2023).
82. Futschek, I. E., Schernhammer, E., Haslacher, H., Stögmann, E. & Lehrner, J. Homocysteine—a predictor for five year-mortality in patients with subjective cognitive decline, mild cognitive impairment and Alzheimer’s dementia. *Exp. Gerontol.* **172**, 112045 (2023).
83. Parkhitko, A. A. et al. A genetic model of methionine restriction extends *Drosophila* health- and lifespan. *Proc. Natl Acad. Sci.* **118**, e2110387118 (2021).
84. Hung, C. C., Chang, C. C., Huang, C. W., Nouchi, R. & Cheng, C. H. Gut microbiota in patients with Alzheimer’s disease spectrum: a systematic review and meta-analysis. *Aging* **14**, 477–496 (2022).
85. Saji, N. et al. Analysis of the relationship between the gut microbiome and dementia: a cross-sectional study conducted in Japan. *Sci. Rep.* **9**, 1008 (2019).
86. Mateo, D., Marqués, M., Domingo, J. L. & Torrente, M. Influence of gut microbiota on the development of most prevalent neurodegenerative dementias and the potential effect of probiotics in elderly: a scoping review. *Am. J. Med. Genet. Part B Neuropsychiatr. Genet.* **195**, e32959 (2024).
87. Wu, L. et al. Altered gut microbial metabolites in amnesic mild cognitive impairment and Alzheimer’s disease: signals in host–microbe interplay. *Nutrients* **13**, 228 (2021).
88. Zheng, J. et al. Stable isotope labeling combined with liquid chromatography-tandem mass spectrometry for comprehensive analysis of short-chain fatty acids. *Anal. Chim. Acta* **1070**, 51–59 (2019).
89. Oakley, H. et al. Intraneuronal  $\beta$ -amyloid aggregates, neurodegeneration, and neuron loss in transgenic mice with five familial Alzheimer’s disease mutations: potential factors in amyloid plaque formation. *J. Neurosci.* **26**, 10129–10140 (2006).
90. Sterniczuk, R., Antle, M. C., Laferla, F. M. & Dyck, R. H. Characterization of the 3xTg-AD mouse model of Alzheimer’s disease: part 2. Behavioral and cognitive changes. *Brain Res.* **1348**, 149–155 (2010).

91. Differding, M. K. et al. Potential interaction between timing of infant complementary feeding and breastfeeding duration in determination of early childhood gut microbiota composition and BMI. *Pediatr. Obes.* **15**, e12642 (2020).
92. Chénard, T., Malick, M., Dubé, J. & Massé, E. The influence of blood on the human gut microbiome. *BMC Microbiol.* **20**, 44 (2020).
93. Yu, Z., García-González, R., Schanbacher, F. L. & Morrison, M. Evaluations of different hypervariable regions of archaeal 16S rRNA genes in profiling of methanogens by Archaea-specific PCR and denaturing gradient gel electrophoresis. *Appl. Environ. Microbiol.* **74**, 889–893 (2008).
94. Yu, Z. & Morrison, M. Improved extraction of PCR-quality community DNA from digesta and fecal samples. *Biotechniques* **36**, 808–812 (2004).
95. Yu, Z., Yu, M. & Morrison, M. Improved serial analysis of V1 ribosomal sequence tags (SARST-V1) provides a rapid, comprehensive, sequence-based characterization of bacterial diversity and community composition. *Environ. Microbiol.* **8**, 603–611 (2006).
96. Caporaso, J. G. et al. Ultra-high-throughput microbial community analysis on the Illumina HiSeq and MiSeq platforms. *ISME J.* **6**, 1621–1624 (2012).
97. Kozich, J. J., Westcott, S. L., Baxter, N. T., Highlander, S. K. & Schloss, P. D. Development of a dual-index sequencing strategy and curation pipeline for analyzing amplicon sequence data on the MiSeq Illumina sequencing platform. *Appl Environ. Microbiol.* **79**, 5112–5120 (2013).
98. Callahan, B. J., McMurdie, P. J. & Holmes, S. P. Exact sequence variants should replace operational taxonomic units in marker-gene data analysis. *ISME J.* **11**, 2639–2643 (2017).
99. Paulson J. N. et al. metagenomeSeq: *Statistical Analysis for Sparse High-Throughput Sequencing*, <<http://www.cbcb.umd.edu/software/metagenomeSeq>> (2013).
100. Paulson, J. N., Stine, O. C., Bravo, H. C. & Pop, M. Differential abundance analysis for microbial marker-gene surveys. *Nat. Methods* **10**, 1200–1202 (2013).
101. McMurdie, P. J. & Holmes, S. phyloseq: an R package for reproducible interactive analysis and graphics of microbiome census data. *PLOS ONE* **8**, e61217 (2013).
102. Bolyen, E. et al. Reproducible, interactive, scalable and extensible microbiome data science using QIIME 2. *Nat. Biotechnol.* **37**, 852–857 (2019).
103. Lin, H. & Peddada, S. D. Analysis of microbial compositions: a review of normalization and differential abundance analysis. *NPJ Biofilms Microbiomes* **6**, 60 (2020).
104. Law, C. W. et al. A guide to creating design matrices for gene expression experiments. *F1000Res* **9**, 1444 (2020).
105. Ritchie, M. E. et al. limma powers differential expression analyses for RNA-sequencing and microarray studies. *Nucleic Acids Res* **43**, e47 (2015).
106. Douglas, G. M. et al. PICRUSt2 for prediction of metagenome functions. *Nat. Biotechnol.* **38**, 685–688 (2020).
107. Yang, C. et al. ggpicrust2: an R package for PICRUSt2 predicted functional profile analysis and visualization. *Bioinformatics* **39**, <https://doi.org/10.1093/bioinformatics/btad470> (2023).
108. Charan, J. & Kantharia, N. D. How to calculate sample size in animal studies? *J. Pharm. Pharmacother.* **4**, 303–306 (2013).

## Acknowledgements

We thank the platform of transcriptomic analysis (“RNomique”) of the Faculté de Médecine et des Sciences de la Santé at the Université de Sherbrooke for the 16S rRNA sequencing. This work was funded by operating grants to K.J.L.F. from the Canadian Institutes of Health Research (CIHR), the Natural Sciences and Engineering Research Council (NSERC), and a Tier 1 Canada Research Chair. E.M. holds grant from the CIHR [MOP389354]. P.E.H.M. was supported by the Bourse d’exemption from the Department of Neurosciences at the Université de Montréal.

## Author contributions

P.E.H.M. developed the concept, carried out the experiments, collected samples, analyzed data, and wrote the manuscript. M.A. and I.S. performed bioinformatic analysis. E.N.K.L. and K.P. extracted DNA and supervised 16S rRNA sequencing. M.M. and A.A. collected samples and performed metabolic monitoring. P.B. analyzed data. E.M. supervised 16S rRNA sequencing, analyzed data and revised the manuscript. K.J.L.F. developed the concept, analyzed data, and revised the manuscript. All authors read and approved the final manuscript.

## Competing interests

The authors declare no competing interests.

## Additional information

**Supplementary information** The online version contains supplementary material available at <https://doi.org/10.1038/s42003-025-09171-9>.

**Correspondence** and requests for materials should be addressed to Eric Massé or Karl J. L. Fernandes.

**Peer review information** *Communications Biology* thanks the anonymous reviewers for their contribution to the peer review of this work. Primary Handling Editor: Benjamin Bessieres.

**Reprints and permissions information** is available at <http://www.nature.com/reprints>

**Publisher’s note** Springer Nature remains neutral with regard to jurisdictional claims in published maps and institutional affiliations.

**Open Access** This article is licensed under a Creative Commons Attribution-NonCommercial-NoDerivatives 4.0 International License, which permits any non-commercial use, sharing, distribution and reproduction in any medium or format, as long as you give appropriate credit to the original author(s) and the source, provide a link to the Creative Commons licence, and indicate if you modified the licensed material. You do not have permission under this licence to share adapted material derived from this article or parts of it. The images or other third party material in this article are included in the article’s Creative Commons licence, unless indicated otherwise in a credit line to the material. If material is not included in the article’s Creative Commons licence and your intended use is not permitted by statutory regulation or exceeds the permitted use, you will need to obtain permission directly from the copyright holder. To view a copy of this licence, visit <http://creativecommons.org/licenses/by-nc-nd/4.0/>.

© The Author(s) 2025